REVIEW

National Science Review
2: 329–348, 2015
doi: 10.1093/nsr/nwv037
Advance access publication 12 July 2015

MATERIALS SCIENCE

Interfaced heterogeneous nanodimers

Yugang Sun

ABSTRACT

Dimerization of different nanocomponents in single nanoparticles becomes interesting due to not only inheritance of properties of both components but also generation of new properties associated with strong coupling of the two components. As a class of emerging nanomaterials, interfaced heterogeneous nanodimers (IHNDs) are attracting more attentions in the field of materials research, in particular, nanoscience and nanotechnology. This review provides a timely and comprehensive overview on the general principles for the synthesis of IHNDs and typical examples of IHNDs made of various compositional combinations. The current challenges related to the synthesis and characterization of IHNDs are summarized at the end of the review and future research directions are also discussed.

Keywords: nanoparticles, nanodimers, hybrid nanostructure, heterogeneous nucleation/growth

INTRODUCTION

Nanoparticle synthesis is one of the most important research topics in nanoscience and nanotechnology since availability of appropriate nanomaterials represents the foundation for exploring novel properties and applications associated with the nanometer length scale. For example, nanoparticles of IB noble metals (e.g. Au and Ag) with various well-controlled sizes and morphologies have been extensively synthesized to demonstrate the tunability of surface plasmon resonance (SPR) in a broad spectral range from ultraviolet (UV) to infrared (IR) [1–3]. In addition, the metal nanoparticles with different compositions can be assembled into compositionally asymmetric dimers through specific linker molecules, leading to the observation of new optical modes that cannot be achieved from either single-component nanoparticles [4]. The new optical signals, such as the normally forbidden out-of-phase mode, originate from the coupling of two different nanoparticles in each dimer, which becomes stronger as the interparticle separation is smaller [5]. The ultimate scenario is that the two nanoparticles in each dimer are bonded each other without assistant of any linkers to form a direct interface (Fig. 1). Such nanoparticulate dimers are defined as 'interfaced heterogeneous nanodimers' (IHNDs) in this review although other names including Janus particles, dumbbell-like particles have also appeared in the literature. Strong coupling of the two different nanoparticles in IHNDs usually leads to novel properties. For instance, we have developed a seed-mediated, surface-confined epitaxial overgrowth strategy to synthesize high-quality Au–Ag IHNDs in the quantum size regime (diameters <10 nm), in which the common face-centered cubic lattices and the nearly identical lattice constants in Au and Ag facilitate epitaxial overgrowth and allow direct contact between the Au and Ag domains [6]. Formation of the Au/Ag interfaces leads to an unusual enhancement of the characteristic Au SPR and the emergence of a charge transfer plasmon across the Au/Ag domains, which together lead to broadband absorption spanning visible to near-IR wavelengths in either Au or Ag domains. Such extended absorption makes the Au/Ag IHNDs a possible class of photocatalysts with efficient utilization of visible light and high surface area associated with their small sizes.

Metal nanoparticles can form IHNDs with semiconductor nanostructures to influence the typical optical and electronic properties of the semiconductor nanodomains. A class of extensively studied examples are nanorods of CdSe and/or CdS with metal tips on either one or both ends of each nanorod, which are synthesized through a room-temperature reaction of semiconductor nanorods with $AuCl_3$ in toluene [7,8]. The direct Au/CdSe interface greatly

Center for Nanoscale Materials, Argonne National Laboratory, Argonne, IL 60439, USA

E-mail: ygsun@anl.gov

Received 10 May 2015; **Accepted** 1 June 2015

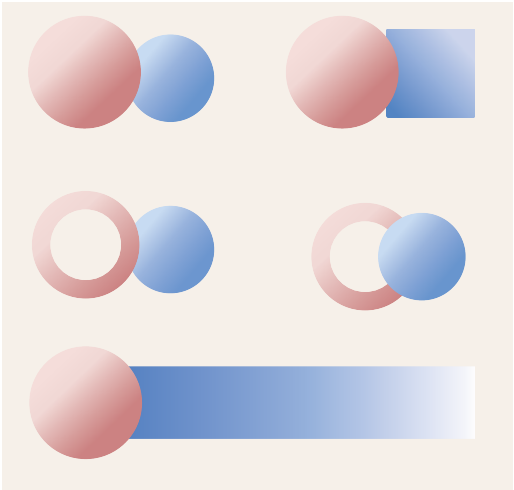

Figure 1. Schematic illustration of IHNDs of two different nanodomains with different compositions and morphologies. The interface formed from the direct contact between the two nanodomains in individual dimers represents the important feature of the IHNDs.

increases (by 1000 000 times) the conductance of individual CdSe nanorods in comparison with pristine CdSe nanorods when they are electrically connected with lithographically defined Au electrodes [9]. Low-temperature tunneling and high-temperature thermionic emission across the junctions at the Au electrodes reveal a significantly lower interface barrier to electric conduction associated with the localized surface states residing near the Au/CdSe interface [10]. The interfaced Au/CdSe and Au/CdS hybrid nanorods exhibit optical responses different from individual materials due to the proximity coupling at the metal/semiconductor interfaces. The CdS nanorods with single-tipped Au nanoparticles (i.e. matchstick-shaped hybrids) essentially retain the absorption properties of their corresponding original components, i.e. the absorption spectrum of the hybrids is a linear combination of that of the CdS nanorods and Au nanoparticles with a minor change. In contrast, the CdSe nanorods with double-tipped Au nanoparticles (i.e. dumbbell-shaped hybrids) exhibit significant changes in absorption properties: the absorption spectra of the CdSe nanorods with small Au tips still show the excitonic structure, but with increased absorbance in the visible spectral region and the appearance of a tail to the red side; the absorption features of the CdSe nanorods are washed out and the tail to the red side becomes more prominent as the Au tips become large in size. Such spectral variation is ascribed to the strong mixing of the semiconductor (CdSe) and metal (Au) electronic states, which leads to modified density of states exhibiting broadened levels and a reduced band gap [11]. When the Au/CdSe hybrid structures dispersed on a substrate consisting of an insulator layer on a conducting surface are excited with photoillumination, they exhibit negative charging that is in contrast with the corresponding individual CdSe nanorods and Au nanoparticles that show positive charging. The different charging behavior revealed by electrostatic force microscopy is ascribed to the strong charge separation in the Au/CdSe hybrid structures, in which the excited electrons are transferred from the CdSe nanorods to the Au tips and the leftover holes in the CdSe nanorods are subsequently filled through tunneling interactions with the substrate [12]. The light-induced negatively charged state can persevere in the hybrid structures for over one hour, even after the photoillumination has been terminated. This charge retention is beneficial for activating photocatalytic activity of the Au/CdSe dumbbell structures in the dark. The number of retained electrons in each Au/CdSe hybrid structure is roughly estimated to be ∼50 after 30 min of photoillumination [13]. The retained electrons can actively reduce methylene blue in anaerobic aqueous solutions in dark while the pre-irradiated CdSe nanorods and Au nanoparticles show much lower photocatalytic activity. The differences in optical responses and the consequential photocatalyic activity between the Au/CdSe hybrid nanostructures and the counterpart single-component nanostructures (i.e. CdSe nanorods and Au nanoparticles) clearly demonstrate the important role of the direct Au/CdSe interfaces in determining unique properties of the hybrid structures.

Metal nanoparticles have also been integrated with magnetic (e.g. Fe_3O_4) nanoparticles to form IHNDs through epitaxial overgrowth of iron oxide on seed metal nanoparticles. The resulting IHNDs always exhibit bimodal functions corresponding to the two individual components. For example, the Au/Fe_3O_4 IHNDs show both the characteristic surface absorption of Au and the magnetic properties of Fe_3O_4 [14]. They also exhibit excellent catalytic activity toward reduction of nitrophenols corresponding to the Au nanodomains and high magnetization corresponding to the Fe_3O_4 that can facilitate recycling of the IHND catalysts [15]. The properties and performance of individual domains are usually influenced by the other domains due to the direct metal/Fe_3O_4 interfaces. The presence of Au enables the Fe_3O_4 in the Au/Fe_3O_4 IHNDs to be active for electrocatalytic reduction of H_2O_2 because of the partial charge transfer at the Au/Fe_3O_4 interface [16]. The similar IHNDs consisting of $Pt_{48}Pd_{52}$ and Fe_3O_4 nanodomains exhibit a much higher activity towards H_2O_2 reduction reaction, leading to a potential for H_2O_2 sensing with a detection limit of 5 nM that is suitable for monitoring

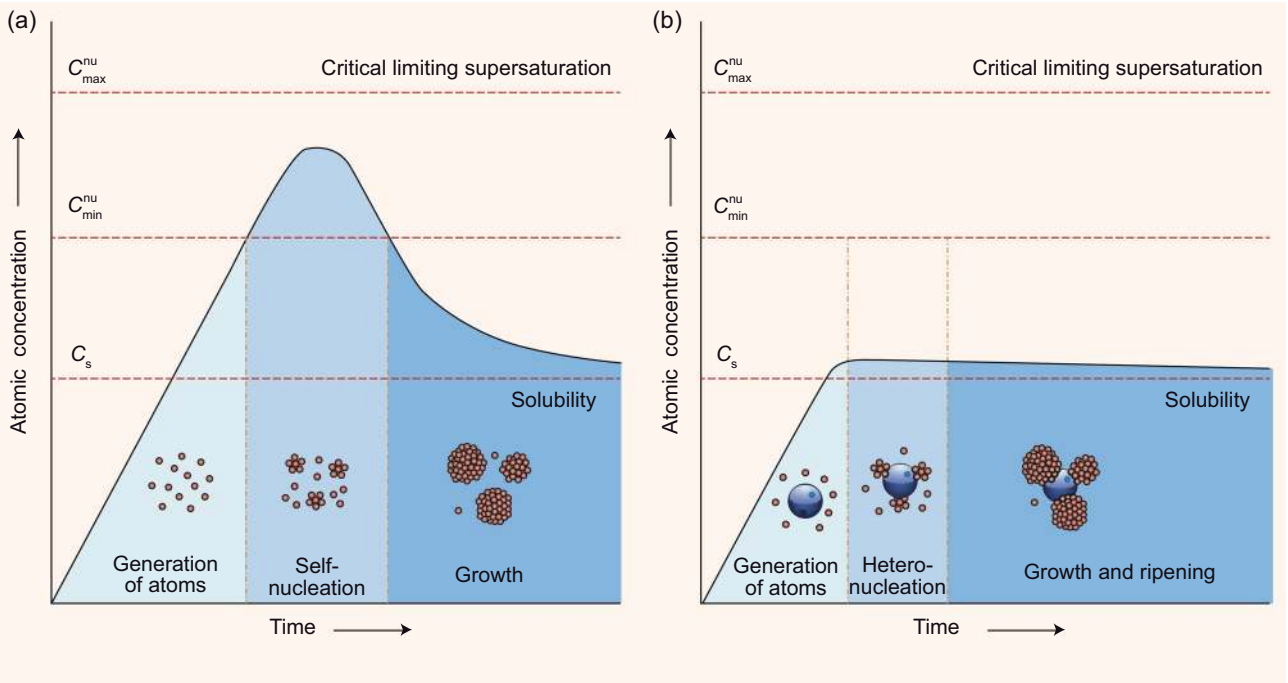

Figure 2. Reaction coordinate diagrams involved in the formation of nanoparticles through (a) homogeneous nucleation and (b) heterogeneous nucleation. C_s represents the saturated concentration of precursor atoms in the reaction solution at the reaction conditions. C^{nu}_{min} and C^{nu}_{max} indicate the bottom limit (minimum) and the top limit (maximum) concentrations, respectively, that determine the range of supersaturation of precursor atoms. The supersaturation is responsible for the spontaneous condensation of precursor atoms into solid nuclei, i.e. self-nucleation. The homogeneous nucleation and growth of nanoparticles shown in (a) can be described with the LaMer model. Adapted with permission from [21]. Copyright 1950, American Chemical Society.

H_2O_2 change in Raw 264.7 cells [17]. In addition to intracellular detection, the $Pt_{48}Pd_{52}/Fe_3O_4$ IHNDs modified with oleylamine-poly(ethylene glycol) have been successfully applied to quantitatively monitor the extracellular H_2O_2 pool generated by mouse neutrophils upon the stimulation of phorbol 12-myristate 13-acetate, demonstrating the potential of these IHNDs as a new class of catalysts to mimic peroxidase for sensitive *in situ* detection of H_2O_2 [18]. On the other hand, the Fe_3O_4 domains can enhance catalytic performance of the metal domains in useful reactions, for example, gas-phase CO oxidation to CO_2 catalyzed by Au/Fe_3O_4 IHNDs [19] and oxygen reduction reaction in alkaline solution catalyzed by Pt/Fe_3O_4 IHNDs [20]. The aforementioned examples clearly show that synthesis of IHNDs represents an interesting and important research direction to achieve materials with unique properties and enhanced performance in applications as well as that IHNDs made of various combinations (e.g. metal–metal, metal–semiconductor, and metal–oxide) can be synthesized through colloidal chemistry.

In this review, the IHNDs synthesized through colloidal chemistry in the past decade are summarized and the general principles for the rational design and synthesis of IHNDs are discussed. The classic nucleation theory is first discussed and seed-mediated heterogeneous nucleation/growth is highlighted to be the efficient strategy for synthesizing IHNDs. Since the overgrown materials require different atomic orderings depending on their crystallinity (i.e. highly crystalline structure versus amorphous structure), hybrid nanostructures with various geometric configurations (e.g. core/shell, IHND, and raspberry-like structure) are produced upon thermodynamic equilibrium. With respect to the combination of seed nanoparticles and overgrown materials (i.e. amorphous/amorphous, crystalline/amorphous, amorphous/crystalline, and crystalline/crystalline), applicable synthetic methods are discussed along with the presentation of typical examples. A brief conclusion and personal perspectives regarding the future directions are provided in the final section to wrap up the review.

SEED-MEDIATED SYNTHESIS OF COLLOIDAL NANOPARTICLES

In general, formation of colloidal nanoparticles in a solution phase follows the model presented by LaMer and Dinegar in 1950, and the model is summarized in Fig. 2a [21]. According to this model,

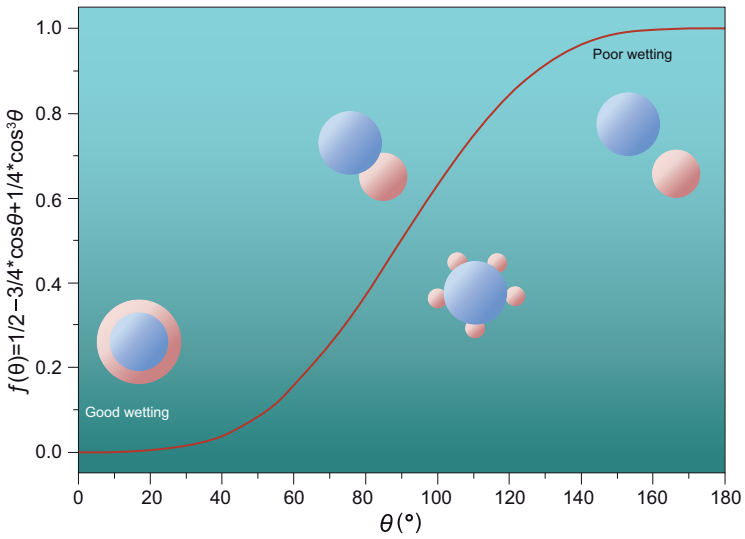

Figure 3. The dependence of $f(\theta)$ on the contact angle, θ, between the new overgrown material (red) and the seed nanoparticles (blue). The large contact angles correspond to poor wetting between the two materials, leading to large heterogeneous nucleation energy barriers to overgrow the new material on the seed nanoparticles. The small contact angels correspond to good wettability between the two materials, leading to low heterogeneous nucleation energy barriers to overgrow the new material on the seed nanoparticles.

a desirable chemical reaction is first triggered to produce precursor atoms in a reaction solution. As long as more atoms are generated, the solution is quickly saturated with the precursor atoms. Even at the saturation concentration (C_s), the atoms are still difficult to spontaneously condense into solid nuclei because forming a new solid phase in the homogeneous solution environment is an energy-consuming process and requires a high chemical potential. As a result, the precursor atoms can condense to form nuclei only when their concentration is supersaturated. Once stable nuclei are formed, they can quickly grow larger at a lower concentration of the precursor atoms that is slightly above the saturation concentration because this process is a less energy-consuming process or an energy-saving process. The significant difference in concentration of precursor atoms required for homogeneous nucleation and particle growth benefits the separation of nucleation and growth steps, enabling the synthesis of highly uniform nanoparticles rather than hybrid nanostructures shown in Fig. 1.

The energy landscape can be significantly changed if nucleation occurs in a solution containing pre-synthesized nanoparticles through the so-called heterogeneous nucleation (Fig. 2b). If the new overgrown material can wet with the seed nanoparticles, supersaturation of precursor atoms is not required for nucleation of the overgrown material. The new material can condense on the seed nanoparticles at a concentration much lower than the supersaturated concentration required for homogeneous nucleation, leading to the formation of interfaced hybrid nanostructures. If there is only one domain of the new material formed on each seed nanoparticle, IHNDs are synthesized in large quantity. The wettability between the seed nanoparticles and the overgrown material is determined by the corresponding contact angle (θ), which is less than 180° when heterogeneous nucleation is promoted on the surfaces of the seed nanoparticles. The free energy barrier required for heterogeneous nucleation equals the product of homogeneous nucleation and a function of the contact angle:

$$\Delta G_{\text{heterogeneous}} = \Delta G_{\text{homogeneous}} \times f(\theta),$$

where

$$f(\theta) = \frac{1}{2} - \frac{3}{4}\cos\theta + \frac{1}{4}\cos^3\theta.$$

As shown in Fig. 3, the energy barrier for nucleation becomes similar to that for homogeneous nucleation when the contact angle is high (>150°, corresponding to a poor wettability). Such high-energy barrier results in a difficulty in promoting heterogeneous nucleation, leading to the formation of separated nanoparticles. In contrast, the energy barrier for heterogeneous nucleation becomes very low (near zero) when the contact angle is low (<30°, corresponding to an extremely good wettability), leading to easy heterogeneous nucleation and formation of core/shell nanoparticles. When the contact angle falls in the range of 30°–150°, heterogeneous nucleation occurs at preferential sites (such as phase boundaries and surface defects) of the seed nanoparticles to lower the overall surface energy. Depending on the reaction conditions, single-site or multiple-site nucleation can be initiated on each seed nanoparticle, leading to the formation of IHNDs or raspberry-like hybrid structures.

In general, solid materials can be classified into crystalline materials and amorphous materials depending on the ordering of atoms. For example, the raw black diamond beads formed in nature exhibit core/shell geometry with highly crystalline diamond cores and amorphous black carbon shells. The positions of carbon atoms in the amorphous carbon shells are not well defined and the interatomic distance can be stretched to conformally surround the crystalline diamond. However, the crystalline diamond cannot conformally cover amorphous black carbon since the relative positions of carbon atoms in diamond are fixed. If the interatomic distance in diamond is stretched, the diamond no longer exists due to lose of its crystallinity.

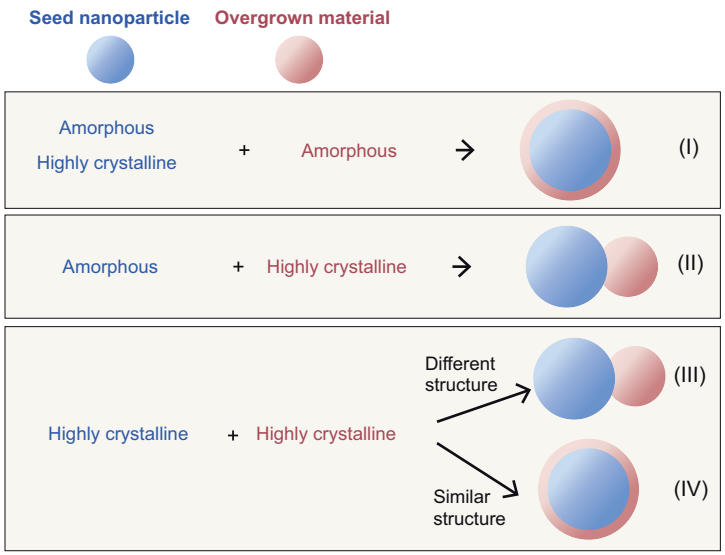

Figure 4. Possible products (either core–shell nanoparticles or IHNDs) formed from different combinations of seed nanoparticles and overgrown materials.

Similarly, overgrowing an amorphous material on seed nanoparticles regardless of their crystallinity tends to form core/shell nanoparticles if the overgrown material wets with the seed nanoparticles (Fig. 4, I). In order to force the overgrown amorphous material to deposit only on partial surfaces of the seed nanoparticles, partial surfaces of the seed nanoparticles can be chemically modified to become non-wetting towards the overgrown material or physically passivated with other inert materials to block the access of the overgrown material (see the sections 'AMORPHOUS/AMORPHOUS IHNDS' and 'Overgrowth of amorphous materials on highly crystalline seed nanoparticles'). If the synthesis is carried out by adding precursors in a reverse order, i.e. overgrowing a highly crystalline material on amorphous seed nanoparticles, the preferential product is seed nanoparticles decorated with individual crystalline nanodomains (Fig. 4, II). Formation of conformal shells is prevented in this case because the interatomic distance in the crystalline overgrown material cannot be freely stretched to accommodate the random atomic orders in the amorphous seed nanoparticles. The number of crystalline domains in each hybrid particle can be controlled by tuning the number of active nucleation sites on each seed nanoparticle. IHND can be synthesized if the number is 1. If the number is larger than 1, IHND can also be achieved through intraparticle Ostwald ripening process, in which the multiple crystalline domains can diffuse on the surface of the seed nanoparticle to coalesce into a single crystalline domain with an increased size. Typical examples are summarized in the section 'Overgrowth of highly crystalline materials on amorphous seed nanoparticles'. Products with similar geometries can be achieved if a highly crystalline material is overgrown on highly crystalline seed nanoparticles with a crystalline structure significantly different from that of the overgrown material (Fig. 4, III). The large mismatch in crystalline lattices between the seed nanoparticles and the overgrown material is not favorable for the formation of core/shell geometry since otherwise large interfacial energy can be built up associated with interfacial lattice tension. Typical IHNDs consisting of different compositional combinations are summarized in the section 'CRYSTALLINE/CRYSTALLINE IHNDS WITH DISSIMILAR CRYSTALLINE STRUCTURES'. In contrast, core/shell particles represent the dominating products when the overgrown material has a similar crystalline structure (in terms of lattice symmetry and lattice constant) to that of the seed nanoparticles because epitaxial overgrowth of the new material on the surfaces of the seed nanoparticles is strongly promoted (Fig. 4, IV). Similar to the case shown in Fig. 4(I), IHNDs are usually synthesized through physical passivation of partial surfaces of the seed nanoparticles with inert materials (see the section 'CRYSTALLINE/CRYSTALLINE IHNDS WITH SIMILAR CRYSTALLINE STRUCTURES').

AMORPHOUS/AMORPHOUS IHNDs

Overgrowing an amorphous material on amorphous seed nanoparticles is less likely to generate apparent interfacial stress since the atomic networks in the amorphous materials are usually mechanical flexible. As a result, chemical wettability between the overgrown material and the seed nanoparticles represents the major parameter to determine the affinity between them. For example, SiO_2 nanoparticles synthesized through the traditional Stöber sol-gel reaction exhibit hydrophilic surfaces terminated with –OH groups while pristine polystyrene (PS) are usually hydrophobic. In order to form SiO_2/PS IHNDs, partial surfaces of SiO_2 nanoparticles have to be chemically modified to exhibit hydrophobic property. Takahara *et al.* [22] developed a method to partially modify the surface hydroxyl groups of SiO_2 nanoparticles with an alkylsilylation agent (i.e. *n*-octadecyltrimethoxysilane, or ODMS), leading to the formation of amphiphilic surfaces. By taking the advantage of the amphiphilic surface property, a one-step miniemulsion polymerization process shown in Fig. 5 was developed to overgrow PS nanodomains on the modified SiO_2 nanoparticles to produce the SiO_2/PS IHNDs [23]. In a typical synthesis, the amphiphilic SiO_2 nanoparticles

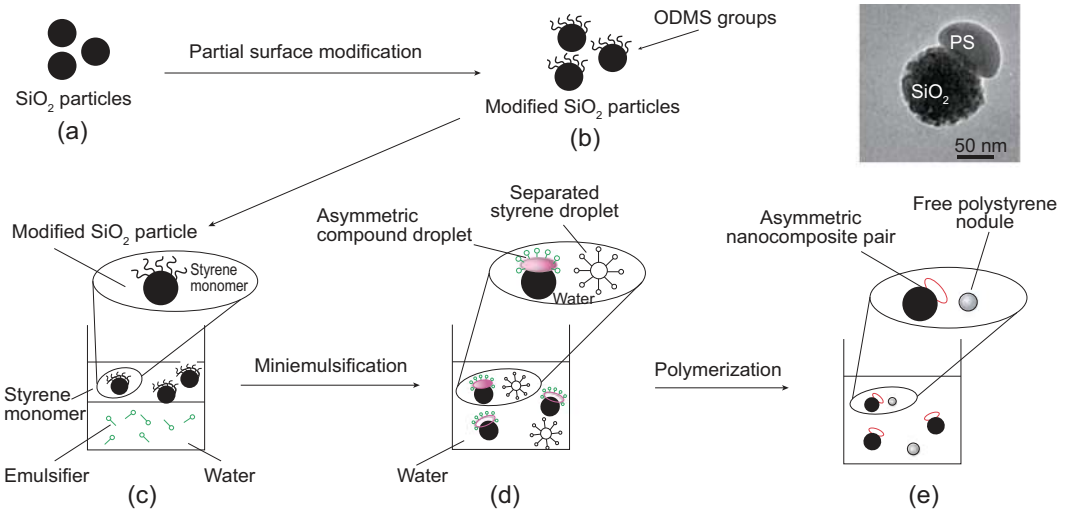

Figure 5. Schematic illustration of the major steps involved in the synthesis of SiO_2/PS IHNDs through a miniemulsion polymerization of styrene monomers on the asymmetrically modified SiO_2 seed particles. PS represents polystyrene. The inset in the top-right corner highlights a TEM image of a synthesized IHND. Adapted with permission from [23]. Copyright 2008, American Chemical Society.

(Fig. 5b) are first dispersed in hexadecane containing styrene monomer to form the oil phase (Fig. 5c, top layer). In deionized water are dissolved surfactant sodium dodecyl sulfate (SDS) and sodium bicarbonate to form the water phase (Fig. 5c, bottom layer). Applying high-power ultrasonication (e.g. 350 W for 20 min) to the system shown in Fig. 5c miniemulsifies the well-separated oil and water phases to form nanometer-sized oil droplets on the hydrophobic SiO_2 surfaces due to the strong hydrophobic–hydrophobic interaction with the styrene monomer molecules (Fig. 5d). Adding water-soluble initiator, potassium persulfate (KPS) to the emulsion triggers the polymerization of styrene monomers in the nanoscale oil droplets at 70°C for appropriate time to form asymmetrical SiO_2/PS IHNDs (Fig. 5e). The inset at the top-right corner of Fig. 5 shows a transmission electron microscopy (TEM) image of a SiO_2/PS IHND with clear interface between the SiO_2 nanoparticle and the PS nodule. Alternatively, partial surfaces of the SiO_2 nanoparticles can be selectively modified in the course of specific emulsion process called Pickering emulsion, which is stabilized by colloidal particles adsorbed onto the oil/water interface [24]. Figure 6a illustrates a scheme including the major steps involved in the synthesis of SiO_2/PS IHNDs via the Pickering emulsion [25]. SiO_2 nanoparticles, styrene monomer, and a small amount of 1-vinylimidazole (1-VID) are mixed with water followed by ultrasonication to form a milky white emulsion. The strong acid–base interaction between hydroxyl groups (acidic) of SiO_2 surfaces and amino groups (basic) of 1-VID enables the SiO_2 nanoparticles to anchor on the surfaces of polymer monomer droplets, leading to formation of stable Pickering emulsion. The surfaces of the SiO_2 nanoparticles exposed to water are then selectively modified with 3-(trimethoxysilyl)propyl methacrylate (MPS) through the reaction of hydroxyl groups of SiO_2 surfaces and methoxy groups of MPS to prevent the polymerization of styrene monomers. When KPS is added to the Pickering emulsion, polymerization is triggered to form PS nanodomains on the SiO_2 nanoparticles without MPS modification. With increase of reaction time, the PS domains are enlarged and connected with the SiO_2 nanoparticles via 1-VID-determined chemical bonds, resulting in the production of SiO_2/PS IHNDs. Figure 6b and c presents typical TEM images of the products synthesized from SiO_2 nanoparticles with different sizes, clearly showing the formation of SiO_2/PS IHNDs. Apparently the strategies shown in Figs 5 and 6 provide the well-defined amphiphilic SiO_2 surfaces to promote the selective polymerization of styrene monomer only on partial surfaces of the SiO_2 nanoparticles, leading to the formation of SiO_2/PS IHNDs with ideal morphology and high yield.

If the hydrophobic surface patches on the SiO_2 nanoparticles cannot be well defined, polymerization of styrene monomer may occur simultaneously at multiple locations of each SiO_2 nanoparticle to form hybrid nanostructure consisting of a SiO_2 nanoparticle decorated with several PS nodules. In the typical seeded emulsion polymerization process,

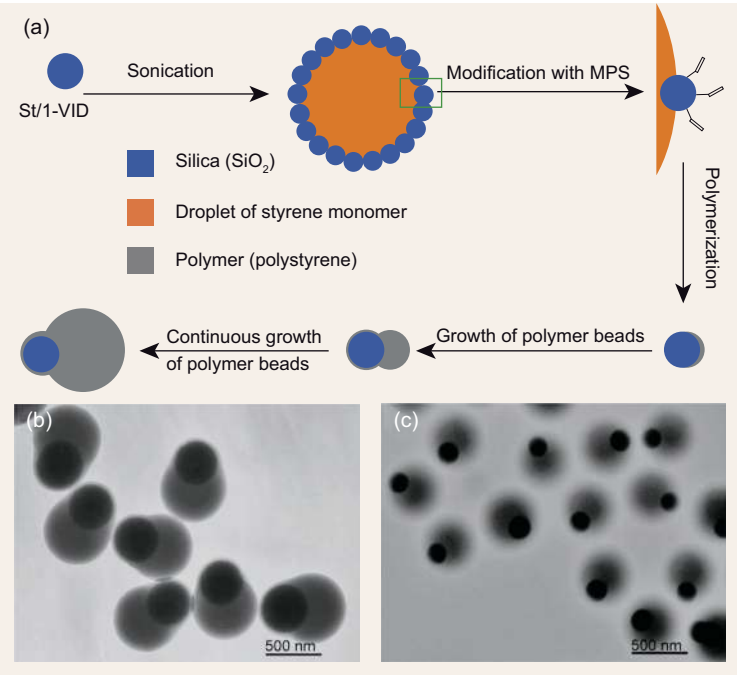

Figure 6. (a) Schematic illustration of the process for synthesizing SiO_2/PS IHNDs through the formation of Pickering emulsion, which provides the anisotropic environment to partially modify the surface of the starting SiO_2 nanoparticles. (b and c) TEM images of the synthesized SiO_2/PS IHNDs by using SiO_2 nanoparticles with 410 nm (b) and 200 nm (c) as seeds, respectively. Adapted with permission from [25]. Copyright 2011, Wiley Periodicals, Inc.

the SiO_2 seed nanoparticles are usually treated with compatibilizers, e.g. poly(ethylene glycol) methacrylate macromonomer [26] and (methacryloxymethyl)triethoxysilane [27,28], in low surface density to create reactive (co)polymerizable loci for growing PS nodules. The number of PS nodules on a single SiO_2 nanoparticle is determined by the competition between two forces, i.e. a repulsive force between the PS nodules that accounts for the presence of negative charges at their surface as they are partially immersed into the aqueous reactive medium, and an attractive force towards the SiO_2 nanoparticle that accounts for the presence of the compatibilizer agent. With introduction of a multiplicative constant K that involves various factors such as the size of the PS nodule, the number of PS nodules, N_{PS}, on each SiO_2 nanoparticle can be described by $\frac{D_{Si}}{2} = K\left(\frac{2N_{PS}}{3} - \frac{1}{2N_{PS}}\right)$, where D_{Si} represents the diameter of the SiO_2 seed nanoparticle [28]. In general, the smaller the PS nodules are, the higher the average number of nodules that can be accommodated on the surface of each SiO_2 nanoparticle. On the other hand, overgrowing SiO_2 onto PS seed nanoparticles requires the selective modification of partial PS surfaces with hydrophilic reagents. For example, immobilizing small iron oxide nanoparticles on the surface of PS nanoparticles can direct the growth of SiO_2 hemisphere on the PS nanoparticles to form PS/SiO_2 IHNDs with the iron oxide embedded in them [29]. Polymerization of both SiO_2 and PS monomer precursors in the same emulsion droplets can also form PS/SiO_2 IHNDs due to the spontaneously phase separation between SiO_2 and PS [30].

AMORPHOUS/CRYSTALLINE IHNDs

An amorphous/crystalline IHND is a dimer consisting of one amorphous domain and one highly crystalline domain that are in direct contact. Synthesis of such IHNDs can start with either amorphous seed nanoparticles or highly crystalline seed nanoparticles, on which either a highly crystalline material or an amorphous material is anisotropically overgrown in a controlled manner.

Overgrowth of amorphous materials on highly crystalline seed nanoparticles

Similar to the overgrowth of an amorphous material on amorphous seed nanoparticles, overgrowing amorphous materials on highly crystalline seed nanoparticles to form IHNDs also requires the selective modification of partial surfaces of the seed nanoparticles. Most documented reports focus on the overgrowth of amorphous materials (e.g. polymer, SiO_2, and TiO_2) on crystalline Au nanoparticles that exhibit unique optical properties associated with strong SPR. The scheme illustrated in Fig. 7a presents a strategy for breaking the symmetry of surface chemistry of Au nanoparticles through modification of the Au surfaces with two competitive ligands exhibiting opposite philicity [31]. For example, mixing Au nanoparticles with both hydrophobic molecules (e.g. 2-dipalmitoyl-*sn*-glycero-3-phosphothioethanol) and hydrophilic molecules (e.g. diethylamine, 2-mercaptoacetic acid, 4-mercaptobenzoic acid) leads to exchanging the original surface ligand (i.e. citrate) of the Au nanoparticles, resulting in the formation of amphiphilic surfaces. The concentration ratio between the hydrophobic and hydrophilic ligand molecules along with their relative binding strength towards the Au surfaces determines the surface ratio between the hydrophobic and hydrophilic patches on the Au nanoparticles. An amphiphilic diblock copolymer (e.g. PS_{154}-*b*-PAA_{60}) is also added to the Au dispersion in the course of surface modification to form micelles on the hydrophobic patches to lower the surface energy by exposing the hydrophilic block PAA_{60} to the surrounding

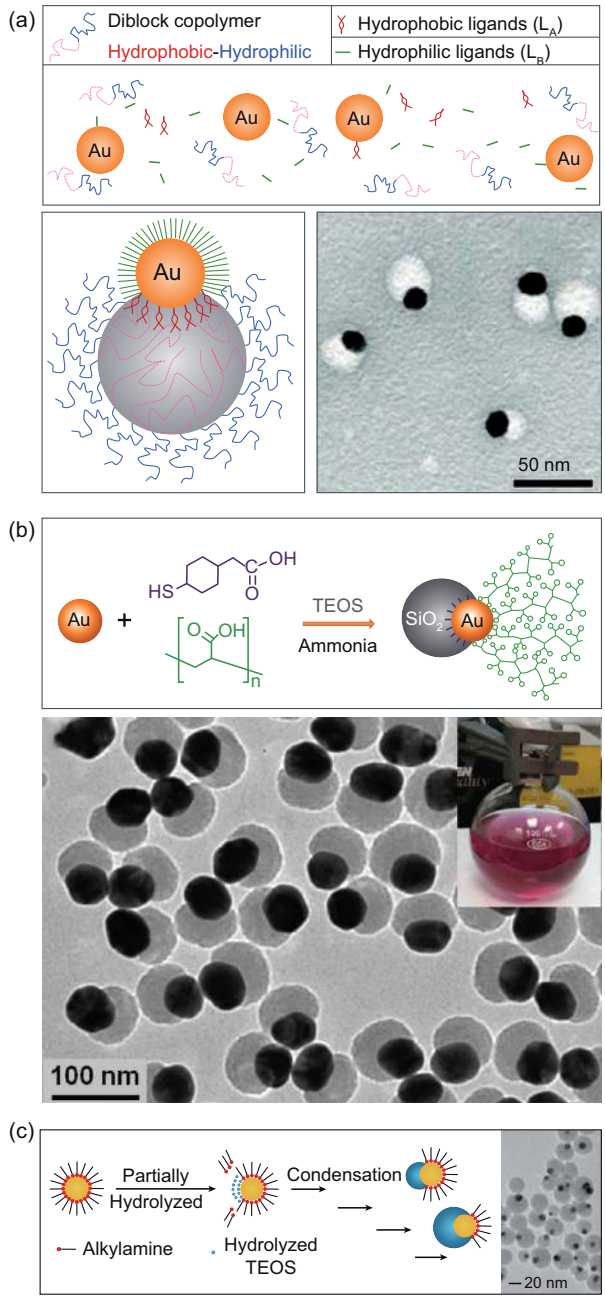

Figure 7. Strategies for the synthesis of crystalline/amorphous IHNDs with the use of Au nanoparticles as the seed nanoparticles. (a) Schematic illustration of the synthesis of Au/polymer IHNDs through the formation of patches from competing hydrophobic and hydrophilic ligands followed by the assembly of hydrophobic–hydrophilic diblock copolymer on the hydrophobic patches. Adapted with permission from [31]. Copyright 2008, American Chemical Society. (b) Schematic illustration of the formation of Au/SiO_2 IHNDs through modification of the Au surfaces with competing ligands. The TEM image shows the corresponding Au/SiO_2 IHNDs synthesized with this strategy, highlighting the high yield of the IHNDs. Adapted with permission from [32]. Copyright 2010, American Chemical Society. (c) Schematic illustration of the mechanism involved in the anisotropic coating of SiO_2 on Au nanoparticles. This synthesis relies on the formation of microemulsion that enables the synthesis of Au/SiO_2 IHNDs in non-polar organic solvents. Adapted with permission from [33]. Copyright 2014, American Chemical Society.

water medium. The aqueous environment forces the hydrophobic PS_{154} blocks to densely pack into PS nodules on the Au nanoparticles, resulting in the formation of Au/PS IHNDs (Fig. 7a, bottom left). Typical TEM images (Fig. 7a, bottom right) of the product formed from the competitive surface modification combining with spontaneous micelle formation clearly show their asymmetric interfaced geometry and heterogeneous compositions. Post-cross-linking of the self-assembled PS_{154} chains may be necessary to harden the PS nodules.

Such competitive ligand exchange also enables the synthesis of Au/SiO_2 IHNDs through the strategy highlighted in Fig. 7b (top). A typical synthesis involves the use of 4-mercaptophenylacetic acid and poly(acrylic acid) (PAA_{86}) as the competing ligands to modify the surfaces of the citrate-stabilized Au nanoparticles in a mixed solvent of 2-propanol and water (5:1, v/v). The Au nanoparticles with patched surfaces can then serve as seeds to mediate heterogeneous nucleation and growth of amorphous SiO_2 through the controlled hydrolysis of tetraethyl orthosilicate (TEOS), resulting in the formation of Au/SiO_2 IHNDs (see the TEM image shown in Fig. 7b, bottom) [32]. However, this method is not suitable for Au nanoparticles synthesized in hydrophobic solvent (e.g. tetradecylamine, or TDA). Chen and co-workers developed a modified water/oil (W/O) microemulsion method similar to that shown in Fig. 5 to selectively grow SiO_2 nanodomains on partial surfaces of the Au nanoparticles [33]. As shown in Fig. 7c, TDA ligand molecules on the Au nanoparticles are partially replaced by the hydrolyzed TEOS molecules, resulting in phase segregation of hydrophobic, aliphatic amine, and hydrophilic TEOS within the emulsion droplets. Continuous condensation of TEOS is confined to the hydrophilic portion of the nanoparticle surface, leading to the formation of Au/SiO_2 IHNDs (see the TEM image shown in Fig. 7c). The higher initial concentration of TEOS can substitute more TDA ligand molecules with the hydrolyzed TEOS to form IHNDs with larger Au/SiO_2 interfaces. Similar approach has also been used to synthesize Au/PS IHNDs by attaching lightly polymerized styrene monomer on partial surface of Au nanoparticles to promote continuous growth of PS nodules [34,35]. Partially replacing cetyltrimethylammonium bromide (CTAB) ligands on Au nanoparticles with hydroxypropyl cellulose that has strong affinity towards TiO_2 is beneficial for the synthesis of Au/TiO_2 IHNDs through controlled hydrolysis of titanium diisopropoxide bis(acetylacetonate) in a 4:1 (v/v) isopropyl alcohol/aqueous solution [36,37].

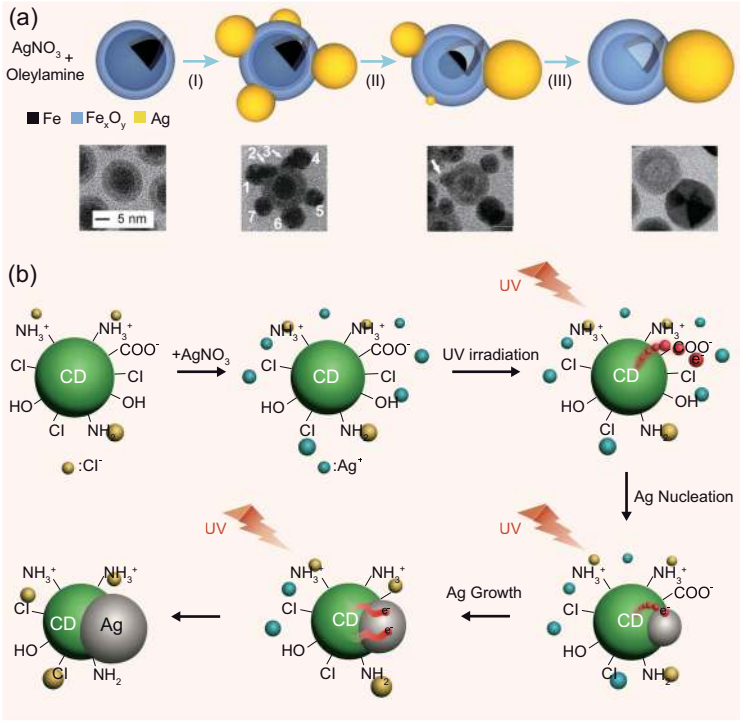

Figure 8. (a) Schematic drawing and the corresponding TEM images of the products formed at different stages involved in the synthesis of amorphous/crystalline Fe_xO_y/Ag IHNDs with the use of amorphous Fe@Fe_xO_y core–shell nanoparticles as seeds. The synthesis can be realized by chemical reduction of $AgNO_3$ with oleylamine at high temperature in the presence of the amorphous Fe@Fe_xO_y core–shell nanoparticles. The TEM images correspond to the products formed at different reaction times: 0, 2, 30, and 300 s (from left to right) that are normalized against the moment when the $AgNO_3$ precursor solution is injected to the reaction solution. The scale bar applies to all images. Adapted with permission from [38]. Copyright 2011, Wiley-VCH Verlag GmbH & Co. KGaA, Weinheim. (b) Proposed mechanism responsible for the formation of amorphous/crystalline CD/Ag IHNDs by using CDs as seeds. CD represents carbon dot. Adapted with permission from [42]. Copyright 2014, American Chemical Society.

Overgrowth of highly crystalline materials on amorphous seed nanoparticles

The atomically disordered surface of an amorphous nanoparticle usually has multiple high-energy sites promoting surface nucleation of an overgrown material. If the overgrown material is amorphous, the multiple nuclei can grow larger and fuse together into a conformal shell on the seed nanoparticle because forming the core–shell morphology represents the ideal way to lower the overall surface energy. In contrast, the multiple nuclei of a highly crystalline material tend to grow larger independently to form a raspberry-like morphology rather than the core–shell structure since a large amorphous/crystalline interfacial strain can be built up along with the formation of a seamless crystalline shell on an amorphous nanoparticle. For example, quickly reducing silver nitrate ($AgNO_3$) in the presence of amorphous iron@iron-oxide (Fe@Fe_xO_y) core–shell seed nanoparticles leads to the decoration of multiple crystalline Ag nanodomains on each amorphous Fe@Fe_xO_y nanoparticle (Fig. 8a, step I) [38]. The starting amorphous Fe@Fe_xO_y seed nanoparticles are synthesized through a thermal decomposition of $Fe(CO)_5$ in nitrogen-protected 1-octadecene (ODE) containing oleylamine (OAm) followed by partial surface oxidation in ambient environment [39]. The heterogeneous nucleation is initiated by injecting an OAm solution of $AgNO_3$ into a hot ODE-OAm mixed solvent containing the amorphous Fe@Fe_xO_y nanoparticles. Quick reduction of Ag^+ forms Ag nanodomains on the surface of the Fe@Fe_xO_y nanoparticles because the amorphous Fe_xO_y surface provides nucleation sites for Ag. Due to the fast reduction of Ag^+ with hot OAm and the high density of nucleation sites on the amorphous Fe_xO_y surface, this heterogeneous nucleation leads to the formation of multiple Ag domains on the surface of each Fe@Fe_xO_y nanoparticle. After the Ag^+ ions in solution are completely reduced, continuously heating the reaction system facilitates the ripening process of the Ag nanodomains because of the high mobility of Ag atoms on the Fe_xO_y surface at elevated temperatures, resulting in a gradual decrease in the average number of the Ag domains on each Fe@Fe_xO_y nanoparticle (Fig. 8a, step II). The ripening process enlarges the most stable Ag nanodomain on one Fe@Fe_xO_y nanoparticle by consuming the others until a dimer is formed (Fig. 8a, step III). During the ripening process, the iron nanoparticles are converted to hollow iron oxide nanoshells through a complete oxidation of the iron with nitrate ions dissociated from $AgNO_3$, resulting in the formation of IHNDs made of amorphous Fe_xO_y shells and crystalline Ag particles. The insets of Fig. 8a present a series of TEM images of typical particles formed at different reaction stages, matching well with the growth mechanism highlighted in the scheme. These particles are obtained by injecting a $AgNO_3$ solution (0.05 M in OAm, 2.0 mL) into hot (180°C) ODE-OAm (10 mL/0.5 mL) in the presence of amorphous Fe@Fe_xO_y nanoparticles with an average diameter of 14 nm (the most left TEM image), followed by continuous heating for different times, i.e. 2, 30, and 300 s from left to right. TEM images of the sample formed at 2 s reveal that each Fe@Fe_xO_y nanoparticle is decorated with multiple Ag nanodomains, for instance, the hybrid particle presented in Fig. 8a is composed of a Fe@Fe_xO_y particle decorated with seven Ag domains. As the reaction proceeds, the average number of Ag domains on each Fe@Fe_xO_y particle gradually decreases until the IHNDs are formed at 300 s.

Another class of interesting amorphous seed nanoparticles are carbon dot (CD) nanoparticles with strong photoinduced fluorescence. The CD

nanoparticles can be excited with UV light to pump energetic electrons to reduce metal ions (e.g. Ag^+) adsorbed on the nanoparticle surface [40]. Alternatively, metal ions can also be directly reduced with the phenol hydroxyl or amine groups on the surface of the CD nanoparticles at elevated temperatures [41]. Since reduction of metal ions occurs directly on the CD nanoparticles, both processes are favorable for the synthesis of hybrid nanostructures consisting of amorphous CD nanoparticles and crystalline metal nanoparticles with amorphous/crystalline interfaces. CD nanoparticles decorated with multiple Ag nanodomains have been synthesized to demonstrate their capability in enhancing efficiencies of polymer optoelectronic devices (e.g. light-emitting diodes, and solar cells) [40]. If the relative size of the Ag nanodomains against the CD nanoparticles and the surface chemistry of the CD nanoparticles are carefully controlled, CD/Ag IHNDs can be synthesized through the aforementioned reduction reactions [42,43]. For example, Choi *et al.* [42] developed a method for the synthesis of CD/Ag IHNDs with the use of amorphous CD nanoparticles derived from microwave pyrolysis of chitosan or alginate in the presence of a surface passivation agent (ethylenediamine) and a solubilizing additive (HCl). As shown in Fig. 8b, surfaces of the CD nanoparticles are terminated with varying chemical groups including amine, Cl, phenol hydroxyl, and carboxyl. In the presence of HCl, the amine groups react with HCl to form NH_4^+:Cl^- ionic pairs. The strong interaction between the surface Cl^- and the solution Ag^+ can form AgCl complex on the CD surface to prevent the electron transfer from the excited CD nanoparticles to free Ag^+ ions. As a result, the photoreduced Ag atoms nucleate only on partial surface of each CD nanoparticle. Continuous reaction grows the Ag nucleus to form a CD/Ag IHND.

Amorphous/crystalline IHNDs made of polymers and Au nanodomains have also been synthesized through a solution template approach and an approach based on interfacial reactions. The former approach relies on the formation of micelles of amphiphilic block copolymer (e.g. PEO-*b*-PS) in an aqueous solution containing $HAuCl_4$ that can be locally accumulated and sequestered in the PEO corona of the micelles. The concentrated $AuCl_4^-$ ions in the PEO corona are reduced to form Au nanoparticles on the PS nanospheres, producing PS/Au IHNDs [44]. A more generalized method depends on the interfacial reactions (including both polymerization for the formation of polymer domains and reduction of metal ions for the formation of metal domains) occurring at an organic/aqueous liquid interface [45]. For example, dissolving organic monomers (e.g. aniline) and inorganic precursors (e.g. $HAuCl_4$) in an organic solvent (e.g. hexane or toluene) and water, respectively, forms two immiscible solutions, which are gently placed in a glass vial to form a water/oil interface. At an appropriate temperature, the precursors simultaneously react at the water/oil interface for the polymerization of aniline to form amorphous polyaniline (PANi) nanoparticles and for the reduction of $HAuCl_4$ to form Au nanoparticles, resulting in PANi/Au IHNDs.

CRYSTALLINE/CRYSTALLINE IHNDs WITH DISSIMILAR CRYSTALLINE STRUCTURES

Overgrowing a crystalline material on a crystalline seed nanoparticle usually follows a spontaneous heterogeneous epitaxial nucleation and the subsequent growth to strongly bond these two crystalline materials together into the hybrid nanostructure. When the overgrown material and the seed nanoparticles exhibit significantly different crystalline structures and lattice parameters, the crystalline/crystalline interface between these two materials tends to shrink to minimize the interfacial energy originated from the lattice mismatch, leading to the spontaneous formation of IHNDs or raspberry-like structures depending on the number of nuclei formed on an individual seed nanoparticle [46]. For example, Prasad and co-workers observed the formation of metallic/magnetic IHNDs by overgrowing magnetic nanocrystals (e.g. F_3O_4, $MnFe_2O_4$, $CoFe_2O_4$) on crystalline Au seed nanoparticles and metallic/semiconductor IHNDs by overgrowing semiconductor nanocrystals (e.g. PbS, PbSe) on Au nanoparticles [47]. Most recently, Kwon *et al.* [48] used *in situ* synchrotron small- and wide-angle X-ray scattering (SAXS/WAXS) techniques to study the nucleation and growth kinetics involved in the overgrowth of Au on $CoPt_3$ seed nanoparticles by monitoring the transient structural and volumetric change of the nanoparticles. The *in situ* results indicate that the synthesis of a $CoPt_3$/Au IHND involves the formation of an intermediate $CoPt_3$@Au core–shell heterostructure at the early stage of reaction. The formation of the pseudomorphic Au shell induces a distortion of crystalline lattice in the core–shell nanoparticle to exhibit a huge stress of ~2 GPa, which substantially increases the free energy of the core–shell nanoparticle. The strain relaxation of the pseudomorphic Au shell forces the transition from a core-shell to an IHND structure, resulting in the nucleation of a strain-free Au nanodomain on an intermediate $CoPt_3$@Au nanoparticle. The formation

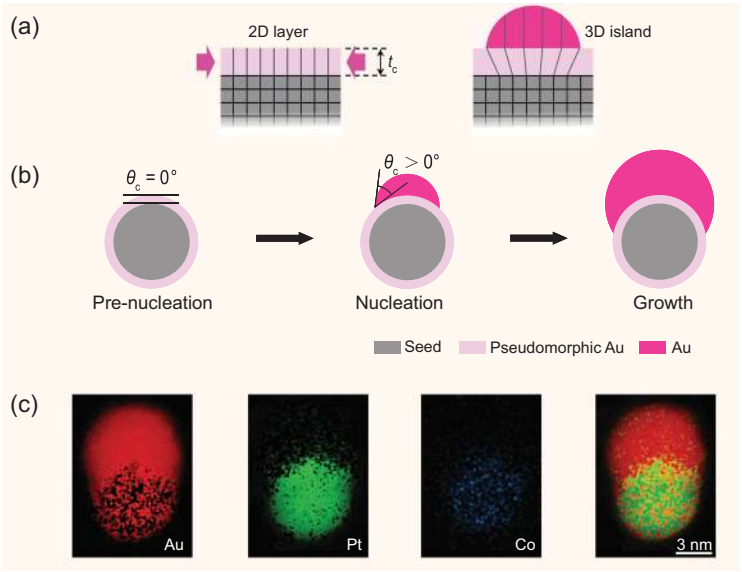

Figure 9. Seed-mediated synthesis of crystalline/crystalline $CoPt_3$/Au IHNDs highlighting the formation of a pseudomorphic Au shell on the $CoPt_3$ seeds. (a) Lattice structure of the overgrown material lattice in the 2D and the 3D mode of the Stranski–Krastanov model. (b) Schematic illustration of the morphological evolution from $CoPt_3$ seed nanoparticles to $CoPt_3$/Au IHNDs through pre-nucleation (formation of a pseudomorphic Au shell), nucleation (formation of an Au island), and growth (formation of an Au nanodomain). The contact angle, θ_c, between the seed and Au represents the indicator for the core/shell ($\theta_c = 0°$) and IHND ($\theta_c > 0°$) geometries. (c) STEM–EDX mapping of a $CoPt_3$/Au IHND at Au M edge (red), Pt M edge (green), and Co L edge (blue). The rightmost image represented the overlaid images of the three elements. Adapted by permission from [48], Copyright 2015, Macmillan Publishers Ltd.

of an intermediate $CoPt_3$@Au core–shell structure is similar to pseudomorphic 2D layer growth on a flat substrate as described in the Stranski–Krastanov model (Fig. 9a) [49]. The overgrown crystalline material usually forms a 2D layer on the substrate if its thickness, t, is smaller than the critical thickness, t_c. Due to the conformal contact of the overgrown lattice with the substrate lattice, the overgrown phase is strained so that its crystal lattice is coherent with the lattice of the substrate (i.e. so-called pseudomorphism), which helps minimizing the lattice mismatch and the interfacial energy. The strain in the overgrown layer increases as its thickness increases. Once it is thicker than t_c, the increased strain energy in the overgrown layer leads to the recovery of the original crystalline structure by dislocation. This change leads to a transition from the pseudomorphic 2D layer to a 3D island (Fig. 9a). Such transition corresponds to the nucleation of an Au nanodomain on an intermediate $CoPt_3$@Au core–shell nanoparticle, and the following continuous growth enlarges the Au nanodomain (Fig. 9b). The existence of an Au shell on the $CoPt_3$ seed nanoparticles is confirmed by energy-dispersive X-ray spectroscopy (EDX)-scanning transmission electron microscopy (STEM) mapping (Fig. 9c). Since the thickness of the Au shell estimated from the SAXS data is 3.2 Å that is comparable to the spatial resolution of the EDX-STEM images, making that the Au shell looks discontinuous in the images. In fact, the Au shell is atomically continuous, which is confirmed by catalytic activity test. The surface of $CoPt_3$ nanoparticles catalyzes hydrogenation reaction of unsaturated hydrocarbon molecules with 100% conversion efficiency [50] while the $CoPt_3$@Au pseudomorphic core–shell nanoparticles cannot catalyze the hydrogenation reaction at all, confirming that the surface of the $CoPt_3$ seed nanoparticles is completely covered with a catalytically inactive Au layer. It is clear that heterogeneous nucleation of a crystalline material on crystalline seed nanoparticles tends to produce IHNDs when these two crystalline materials are immiscible and exhibit different crystalline structures. A number of compositional combinations of crystalline/crystalline IHNDs have been successfully synthesized.

Metal/metal IHNDs with large lattice mismatch

Gold can be overgrown on different metal nanoparticles including $CoPt_3$ nanoparticles shown in Fig. 9 to form metal/metal IHNDs. Pellegrino *et al.* [51] also used $CoPt_3$ nanoparticles as seeds to guide the heterogeneous nucleation and growth of Au nanodomains by dropwise adding a toluene solution of $AuCl_3$, dodecylethyldimethylammonium bromide (DEDAB) and dodecylamine to a colloidal solution of $CoPt_3$ nanoparticles, resulting in the formation of $CoPt_3$/Au IHNDs (Fig. 10a). Structural characterization by high-resolution TEM reveals that both crystalline domains in each $CoPt_3$/Au IHND adopt the same faced-centered cubic (fcc) Bravais lattice and can share a common {111}, {100}, or {110} facet depending on the size of the $CoPt_3$ seed nanoparticles. Au nanodomains can also be overgrown on FePt seed nanoparticles to form FePt/Au IHNDs (Fig. 10b). When FePt nanoparticles are mixed with AuCl-(PPh_3) in 1,2-dichlorobenzene (DCB) containing 1-hexadecylamine, bubbling the solution with a 4% H_2/Ar can trigger the selective reduction of Au^+ to Au^0 on the surface of the FePt nanoparticles since the FePt nanoparticles provide catalytic surface to activate the molecular hydrogen. The selective catalytic reduction facilitates nucleation and successive growth of Au nanodomains on FePt seed nanoparticles [52]. Room-temperature reduction of $AuCl_4^-$ in a DCB solution containing 0.45% OAm and 2.5% 1-undecanol in the presence of Pt seed nanoparticles produces Pt/Au IHNDs

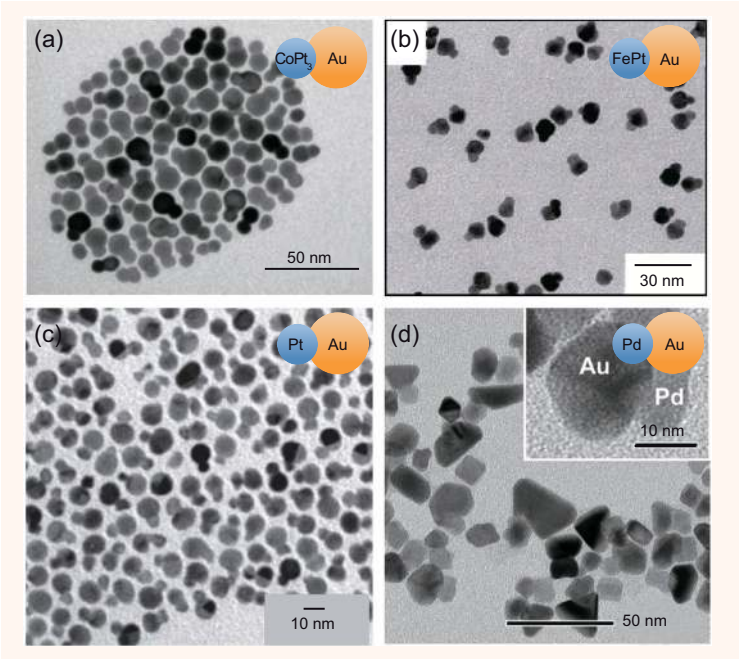

Figure 10. Typical TEM images of metal/metal IHNDs formed by overgrowing Au nanodomains on different metal seed nanoparticles: (a) $CoPt_3$, (b) FePt, (c) Pt, and (d) Pd. (a) Adapted with permission from [51], Copyright 2006, American Chemical Society; (b) Adapted with permission from [52], Copyright 2006, American Chemical Society; (c) Adapted with permission from [53], Copyright 2011, the Royal Society of Chemistry; (d) Adapted with permission from [55], Copyright 2010, American Chemical Society.

(Fig. 10c) [53]. In general, Pt and Au are immiscible and the heterogeneous nucleation/growth tends to form Pt@Au or Au@Pt core–shell nanoparticles at elevated temperatures [48,54]. The formation of Pt/Au IHNDs is possibly due to the redistribution of electronic charges within the Pt seed nanoparticles. Once Au nuclei are formed on particular facets of the Pt seeds, electrons are transferred from Pt to Au between their Fermi levels across the Pt/Au interfaces. The modification of charge distribution in the Pt seeds can compensate for the potential at the Pt/Au interfaces and the rest exposed Pt surfaces become much less effective towards additional Au nucleation, favoring the formation of Pt/Au IHNDs. In addition, the required energy for Au nucleation at room temperature is significantly higher than that for growth, further benefiting the formation of IHNDs. Reduction of $HAuCl_4$ in an aqueous solution containing cubic Pd seeds can form either Pd@Au core–shell nanoparticles or Pd/Au IHNDs (Fig. 10d) depending on the use of different reducing agents, i.e. L-ascorbic acid for core–shell particles and citric acid for IHNDs [55]. In the Pd/Au IHNDs, the Au nanodomains exhibit primarily either partial decahedral or plate-like morphology with their surfaces enclosed by {111} facets, indicating that citric acid may play a profound role in stabilizing the {111} facets of the Au domains. Similar reduction of $AgNO_3$ in the presence of seed nanoparticles with Pd surfaces (e.g. Au@Pd core–shell nanoparticles) can form IHNDs that are composed of the seed nanoparticles and the overgrown Ag nanodomains [56]. Galvanic displacement reaction of shaped Ni nanoparticles preferably nucleates Ag on the vertices of Ni nanopyramids and vertices/edges of Ni nanocubes to form Ni/Ag IHNDs, which exhibit both plasmonic resonance and superparamagnetic behavior [57]. The Ni/Ag IHNDs exhibit a magnetic moment higher than the pristine Ni nanoparticles, suggesting a specific magnetic polarization of the Ni/Ag interface or Ag nanodomains. Chen *et al.* [58] developed a general strategy to overgrow Cu on more noble metal nanoparticles (e.g. M = Au, Pt, or Pd) based on a seeded sequential coreduction method. In a typical synthesis, the noble metal nanoparticles are synthesized through the conventional reduction of corresponding salt precursors in organic solvents (e.g. OAm) at elevated temperatures. To the reaction solution is added Cu precursor (e.g. $Cu(acac)_2$, $CuCl_2$, $Cu(CH_3COO)_2$), and the as-formed noble metal nanoparticles serve as seeds to promote heterogeneous nucleation of Cu to form M/Cu IHNDs. Due to miscibility of Cu with these noble metals, the M/Cu IHNDs are transformed to M/Cu alloys if the reactions last long at elevated temperatures. Coreduction of $HAuCl_4$ and $Ni(NO_3)_2{\cdot}6H_2O$ in octadecylamine, which serves as both the solvent and the surfactant, forms Au/Ni IHNDs [59]. Although both the metal precursors can be reduced, Au nanoparticles should be formed first to serve as seeds for heterogeneous nucleation of Ni because $AuCl_4^-$ exhibits higher reduction potential than Ni^{2+}.

Metal/oxide IHNDs

Metal ions can be selectively reduced on oxide nanoparticles to nucleate and grow into metal/oxide IHNDs. For example, photoreduction of Ag^+ in an ethanediol/water solution containing ZnO nanorods with a monochromatic light (wavelength of 340 nm) results in a selective deposition of spherical Ag nanoparticles at the single ends of the ZnO nanorods, forming ZnO/Ag IHNDs [60]. Another demonstrated example is the heterogeneous nucleation of spherical ε-Co nanodomains on anatase TiO_2 nanorods with selective attachment at either nanorod tips or multiple locations along the nanorod sidewalls depending on reaction conditions. If the heterogeneous nucleation occurs only at one end of each TiO_2 nanorod, TiO_2/Co IHNDs can be synthesized [61]. In

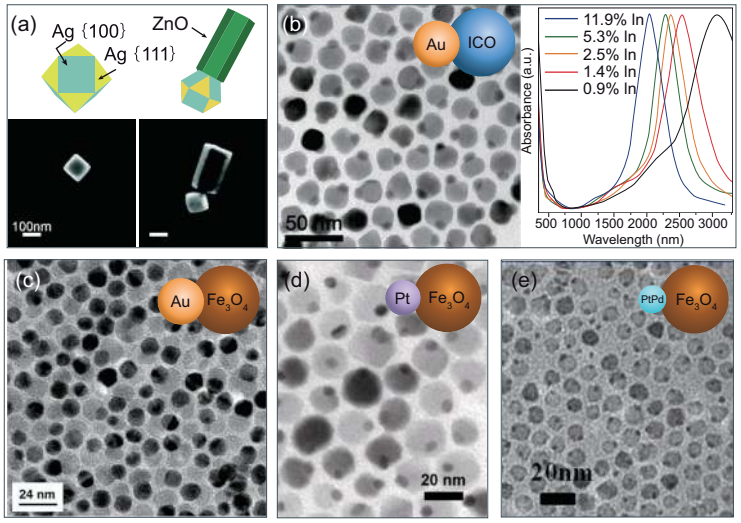

Figure 11. Examples of metal/oxide IHNDs formed by overgrowing oxide nanodomains on different metal seed nanoparticles. The compositional combinations include (a) Ag/ZnO, (b) Au/ICO, (c) Au/Fe_3O_4, (d) Pt/Fe_3O_4, and (e) PtPd/Fe_3O_4. (a) Adapted with permission from [65], Copyright 2009, American Chemical Society; (b) Adapted with permission from [66], Copyright 2014, American Chemical Society; (c) Adapted with permission from [14], Copyright 2005, American Chemical Society; (d) Adapted with permission from [20], Copyright 2009, American Chemical Society; (e) Adapted with permission from [17], Copyright 2012, American Chemical Society.

addition to semiconductor oxides, magnetic oxide nanoparticles have also been used as seeds to synthesize metal/oxide IHNDs. Mixing α-Fe_2O_3 seed nanocrystals with $HAuCl_4$ in an aqueous solution containing L-cysteine and L-ascorbic acid followed by reaction for 3 h under vigorous stirring leads to the formation of raspberry-like structures comprising Fe_2O_3 nanoparticles decorated with multiple 2-nm Au nanocrystals. The as-formed Fe_2O_3/2-nm-Au raspberry hybrid particles are then mixed with SDS in 1:1 (v/v) water/isopropanol solvent. To this dispersion is added dropwise an appropriate amount of aqueous solution of $HAuCl_4$ under illumination of a halogen lamp, leading to the formation of α-Fe_2O_3/Au IHNDs [62]. The reaction conditions in the first step are favorable for heterogeneous nucleation of Au on the surface of the α-Fe_2O_3 nanoparticles while the reaction conditions in the second step accelerate the growth of Au nuclei as well as intraparticle ripening of 2-nm Au nuclei. The differences observed in these two steps highlight the importance of reaction conditions on the formation of well-defined IHNDs. By using Fe_3O_4 and $CoFe_2O_4$ nanocrystals as seeds in hydrophobic solvents, Ying's group and Sun's group have demonstrated the feasibility to overgrow Ag nanodomains on these seeds to synthesize Fe_3O_4/Ag and $CoFe_2O_4$/Ag IHNDs, respectively [63,64]. The as-synthesized hydrophobic Fe_3O_4/Ag IHNDs can be rendered hydrophilic by modifying the Fe_3O_4 surface with hydroxyl groups and the Ag surface with carboxyl and amine bearing thiol molecules, which can be used as a class of unique label for two-photon fluorescence imaging and magnetic manipulation. The $CoFe_2O_4$/Ag IHNDs exhibit a significant enhancement of magnetooptic response outside the $CoFe_2O_4$ interband-dominated spectral regime due to the plasmonic contribution by the Ag nanodomains.

On the other hand, crystalline metal nanoparticles can serve as seeds to promote heterogeneous nucleation of oxide materials to form metal/oxide IHNDs. For instance, in the presence of Ag-truncated nanocubes, growth of colloidal ZnO nanorods prefers to nucleate on {111} rather than {100} facets of the Ag crystalline seeds. Ag/ZnO IHNDs can be synthesized if there is only one ZnO nanorod overgrown on each Ag nanoparticle (Fig. 11a) [65]. In addition to the well-faceted metal nanocrystals, Ye *et al.* [66] have demonstrated the use of isotropic spherical metal nanocrystals (e.g. Au, Pd, Pt, and FePt) as seeds to guide the heterogeneous nucleation of indium-doped cadmium oxide (ICO) that was derived from the thermal decomposition of the cadmium and the indium precursors at reflux temperature (~316°C) of the reaction solution. The rapid nucleation of ICO on the existing metal seeds results in the formation of metal/ICO IHNDs (e.g. Au/ICO IHNDs shown in Fig. 11b, left). The doping concentration of In in the ICO nanodomains can be easily tuned by controlling the molar ratio of the In precursor and the Cd precursor in the reaction solution, which can influence their corresponding optical properties. As shown in Fig. 11b (right), the Au/ICO IHNDs exhibit two distinct plasmon resonances arising from separate dipolar plasmon excitations in the Au (i.e. the peak at ~550 nm) and ICO (i.e. the peak in the near IR range) nanodomains. With variation of the In concentration, the SPR band position of the ICO nanodomains can be tuned from 1.9 to 3.6 μm although the SPR peak position of the Au nanodomains remains essentially constant. The double-peak characteristic of the Au/ICO IHNDs makes them to be the 'optical equivalent' of monodisperse Au nanorods with very high aspect ratio (>10), for which reliable synthesis is still a challenge. Pioneered by Sun and co-workers, the spherical metal nanocrystals of different compositions have also been used to promote heterogeneous nucleation of single crystalline Fe_3O_4 to synthesize metal/Fe_3O_4 IHNDs [67]. The Fe_3O_4 nanodomains are formed from thermal decomposition of $Fe(CO)_5$ in ODE solvent containing oleic acid and OAm at flux temperature (~300°C) followed by room-temperature oxidation

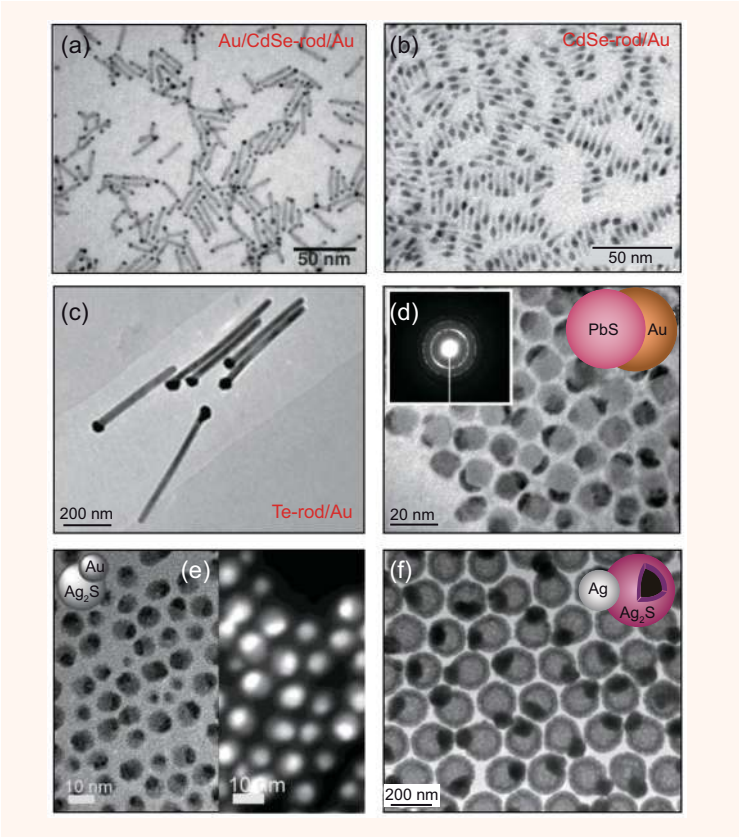

Figure 12. Examples of chalcogenide/metal IHNDs formed through overgrowing noble metal nanodomains on chalcogenide nanostructures. The compositional combinations include (a) Au/CdSe-nanorod/Au, (b) CdSe-nanorod/Au, (c) Te-nanorod/Au, (d) PbS/Au, (e) Ag_2S/Au, and (f) hollow-Ag_2S/Ag. (a) Reprinted with permission from [7], Copyright 2004, AAAS; (b) Reprinted with permission from [8], Copyright 2005, Macmillan Publishers Ltd; (c) Adapted with permission from [77], Copyright 2008, the Royal Society of Chemistry; (d) Adapted with permission from [78], Copyright 2006, American Chemical Society; (e) Adapted with permission from [80], Copyright 2011 Wiley-VCH Verlag GmbH & Co. KGaA, Weinheim; (f) Adapted with permission from [81], Copyright 2010, American Chemical Society.

in air, leading to the formation of Au/Fe_3O_4 (Fig. 11c) [14,68], Pt/Fe_3O_4 (Fig. 11d) [20], and $Pt_{48}Pd_{52}$/Fe_3O_4 IHNDs (Fig. 11e) [17] when Au, Pt, and $Pt_{48}Pd_{52}$ nanoparticles are used as seeds. Heterogeneous nucleation on other metal nanocrystals such as Ag and PeFt is also possible to synthesize IHNDs made of Ag/Fe_3O_4 [69] and FePt/Fe_3O_4 [70].

Metal/chalcogenide IHNDs

Intensive efforts have been devoted to the synthesis and characterization of metal/chalcogenide hybrid nanostructures since the pioneering work entitled 'selective growth of metal tips onto semiconductor quantum rods and tetrapods' was reported by Banin and co-workers in 2004 [7]. In a typical synthesis, CdSe nanorods with different sizes are first synthesized through high-temperature pyrolysis of appropriate precursors in a mixture solvent containing phosphonic acids and trioctylphosphine oxide that also serves as capping ligand to stabilize the as-grown CdSe nanorods. Adding the CdSe nanorods to a toluene solution of $AuCl_3$, dodecyldimethylammonium bromide, and dodecylamine at room temperature spontaneously initiates the redox reaction between $AuCl_3$ and CdSe to selectively nucleate/grow Au nanoparticles on the ends of the CdSe nanorods, leading to the formation of Au/CdSe-rod/Au interfaced dumbbell-like nanostructure (Fig. 12a). The redox reaction consumes CdSe and benefits the growth of Au, which is consistent with the size reduction of the CdSe nanorods and the enlargement of the Au nanoparticles observed in the course of reaction [7]. Their following-up experimental and theoretical work demonstrates that a ripening process can drive the Au nanoparticles from one end to other to transform the Au/CdSe-rod/Au dumbbell nanorods to Au/CdSe-rod IHNDs (Fig. 12b) [8]. This morphological transformation is ascribed to the phase segregation between Au and CdSe, which minimizes the Au/CdSe interfacial area. Such intraparticle ripening has very different consequences in comparison with the more common Ostwald ripening: upon its completion, each hybrid nanostructure contains only one Au tip while coarsening associated with Ostwald ripening results in a decrease in the number of particles, asymptotically, to a single large one. The spatial selectivity for nucleation of Au nanoparticles on the cadmium chalcogenide nanorods (e.g. CdS nanorods and CdSe@CdS nanorods) is sensitive towards reaction temperature because more nanorods' surface defects, on which small Au nanoparticles can nucleate, can be activated at high temperatures [71]. As a result, lowering the reaction temperature can suppress simultaneous nucleation of multiple Au nanoparticles on the surface of each nanorod. This temperature-dependent control is caused by a phase transition of the alkyl chains of the surface amine ligands on the nanorod surface to a static phase at lower temperatures, blocking the Au precursor to access the nanorod surface. Because of their semiconductor characteristics, the chalcogenide nanorods can be photoexcited to generate energetic electrons that migrate to one tip of each nanorod due to the confinement of its anisotropic morphology and crystalline structure. The accumulated energetic electrons can reduce Au ions to selectively grow Au nanoparticle only on one end of each nanorod [72]. Combining photoillumination and low-temperature reaction provides an effective way for a highly selective synthesis of hybrid semiconductor nanorods with single gold tips (i.e.

Au/chalcogenide-nanorod IHNDs similar to that shown in Fig. 12b) [71]. Cozzoli and Manna have demonstrated an alternative way to enhance the selective deposition of Au nanoparticles on the ends of CdSe and CdS nanorods through a two-step approach: (i) a sacrificial material (e.g. PbSe or CdTe) first nucleates at the ends of the nanorods; (ii) these sacrificial tips are then oxidized with Au precursor ions to form Au nanoparticles only at the ends of the nanorods [73]. Metal tips of different compositions (e.g. Ag [74], Pt [75], binary PtNi and PtCo [76]) have also been selectively deposited on the ends of the chalcogenide nanorods. Similar to chalcogenide nanorods, Te nanowires exhibit redox potentials that are low enough to reduce Au precursors to nucleate Au nanoparticles on the surface of the Te nanowires. The redox reaction potential of Te depends on the pH value of the reaction solution, i.e. higher pH lowers the redox potential to accelerate reduction of the Au precursors. By carefully controlling the pH value, reaction of the Te nanowires with $AuCl_4^-$ ions in an aqueous solution containing CTAB leads to the formation of Au/Te-nanowire IHNDs (Fig. 12c) and Au/Te-nanowire/Au dumbbell-like nanostructure at pH of 4 and 5, respectively [77].

Nanocrystals of no-cadmium chalcogenides (e.g. PbS, Ag_2S) are also able to serve as seeds to facilitate overgrowth of metal nanoparticles. For example, injection of a toluene solution of $HAuCl_4$ and capping ligands (including tetraoctylamine bromide and dodecylamine) to a toluene dispersion of PbS nanocrystals triggers the nucleation of Au nanocrystals on the PbS nanocrystals at 40°C under protection of N_2. The number of Au nanocrystals on each PbS nanocrystal depends on the concentration of $HAuCl_4$ in the reaction solution. At a low concentration of $HAuCl_4$ (0.33 mM), only one Au nanocrystal can overgrow on each PbS nanoparticle (i.e. Au/PbS IHNDs as shown in Fig. 12d), whereas PbS nanoparticle can be decorated with multiple Au nanocrystals at increased concentration of $HAuCl_4$ [78]. If the concentration of $HAuCl_4$ is too high, the excessive $HAuCl_4$ can etch the PbS nanoparticles to transform them into hollow particles [79]. Since Au has a stronger imaging contrast than PbS, the formation of Au/PbS IHNDs can be easily identified from the TEM image (Fig. 12d). The overgrown Au covers only one side of the PbS nanocrystals like a cap. The selected area electron diffraction pattern (inset, Fig. 12d) of the Au/PbS IHNDs confirms that both the Au and PbS nanodomains are highly crystalline. Yang and Ying have synthesized hydrophilic Ag_2S nanocrystals through the precipitation reaction between BSPP–Ag^I complexes (that is formed from the mixture of bis(*p*-sulfonatophenyl)phenylphosphane dehydrate dipotassium salt, or BSPP, and $AgNO_3$ in an aqueous solution) and Na_2S in an aqueous solution. The as-synthesized Ag_2S nanocrystals have been used as seeds for heterogeneous nucleation of different metals, which are formed from reduction of their corresponding precursors with sodium citrate at elevated temperatures (e.g. 105°C for Au and 110°C for other metals) [80]. Characterization of the synthesized hybrid nanostructures shows that Au is deposited only at a single site on each Ag_2S nanocrystal to form Au/Ag_2S IHNDs (Fig. 12e) while the nucleation of other metals including Pt, Os, and Ir occurs at multiple sites on each Ag_2S nanocrystal to form raspberry-like nanostructures. Synthesis of Ag/Ag_2S IHNDs (Fig. 12f) has been demonstrated by using hollow Ag_2S nanocrystals as seeds to catalyze heterogeneous nucleation of Ag nanocrystals, which are derived from reduction of Ag^+ with ethanol [81].

There are also a few papers reporting the use of metal nanocrystals as seeds for heterogeneous nucleation of chalcogenides [82,83]. For instance of the synthesis of FePt/PbS hybrid nanostructures, bis(trimethylsilyl) sulfide is injected into an ODE solution containing monodisperse FePt nanocrystals, oleic acid, and Pb-oleate complex. The passivation strength of ligands on the surface of the FePt nanocrystals determines the morphology of the FePt/PbS hybrid nanostructure. When the surface of the FePt nanocrystals, originally stabilized with oleic acid and OAm, is treated with excessive OAm that can strongly bonded to the nanocrystal surface, FePt@PbS core–shell nanostructures are formed since the treatment with labile amine surfactant molecules favors simultaneous nucleation of PbS at multiple sites on the surface of the FePt seeds. In contrast, FePt/PbS IHNDs can be synthesized if the FePt nanocrystals are extensively washed to remove the OAm ligands followed by recapped with less labile oleate ligand [82]. This example clearly demonstrates the importance of the surface passivation on the morphology of the hybrid nanostructures synthesized from seed-mediated heterogeneous nucleation.

IHNDs made of oxides and/or chalcogenides

Non-metal materials, such as oxides and chalcogenides, are also possible to intimately contact each other to form IHNDs although they are not as popular as the IHNDs containing metal nanodomains. Typical examples include oxide/oxide, oxide/chalcogenide, and chalcogenide/chalcogenide combinations. For example,

Cozzoli and co-workers have successfully synthesized TiO_2/γ-Fe_2O_3 IHNDs through heterogeneous nucleation of γ-Fe_2O_3 onto the longitudinal facets of anatase TiO_2 nanorods in an ODE solution containing a ternary surfactant mixture (i.e. OAm, oleic acid, and dodecan-1,2-diol). The heteroepitaxial growth at the TiO_2/γ-Fe_2O_3 interface follows the mechanism, in which both the TiO_2 and the γ-Fe_2O_3 domains share a restricted and locally curved junction region to efficiently accommodate the interfacial strain and prevent the formation of misfit dislocations [84]. When UO_2 nanocrystals are used as seeds in hot ODE reaction solution, thermal decomposition of the indium oxide precursor leads to heterogeneous nucleation of only single In_2O_3 nanocrystal on each UO_2 seed, resulting in the production of UO_2/In_2O_3 IHNDs [85]. The intrinsic structural polarity of ZnO (0001) surface helps heterogeneous nucleation of crystalline TiO_2 nanocrystals selectively on single-end surface of ZnO nanorods to form ZnO/TiO_2 IHNDs [86].

Kwon and Shim have reported a generalized method to form γ-Fe_2O_3/MS (M = Cd, Zn, Hg) hybrid nanostructures using γ-Fe_2O_3 nanocrystals as seeds to promote the deposition of MS shells with low crystallinity [87,88]. Annealing the γ-Fe_2O_3@MS core–shell nanoparticles at elevated temperatures increases the crystallinity of the MS shells along with a transformation of them into individual MS nanocrystals on the surface of the γ-Fe_2O_3 nanoparticles. The number of MS nanocrystals on each γ-Fe_2O_3 nanoparticle depends on the overgrown sulfide materials, for example, γ-Fe_2O_3/ZnS hybrid nanostructures exhibit a raspberry-like morphology with each Fe_2O_3 nanoparticle decorated with two or more ZnS nanocrystals while γ-Fe_2O_3/CdS and γ-Fe_2O_3/HgS exhibit a morphology of IHNDs [87]. Using superparamagnetic Fe_3O_4 nanocrystals as seeds, heterogeneous nucleation of fluorescent CdSe nanocrystals results in the synthesis of Fe_3O_4/CdSe IHNDs that exhibit two attractive features, i.e. fluorescence and superparamagnetism, which enable their movements to be controlled using external magnetic force and to be monitored using a fluorescent microscope. Such bifunctional feature provides an effective way to probe specific functions of bioactive molecules in localized domains or compartments of living cells without disturbing other parts of the cells [89]. Due to the presence of dangling Cd bonds, the end surface of the CdS and CdSe nanorods provides the active sites for the selective nucleation of other chalcogenides, such as PbSe and CdTe, to form chalcogenide/chalcogenide IHNDs [73,90,91].

CRYSTALLINE/CRYSTALLINE IHNDs WITH SIMILAR CRYSTALLINE STRUCTURES

When the overgrown material has similar crystalline structure to the seed nanoparticles in terms of lattice symmetry and lattice constant, epitaxial overgrowth of the new lattice on the seed nanoparticles does not build up significant interfacial stress, guiding the formation of core–shell nanostructures. A typical example is the overgrowth of Ag on Au nanoparticles or reverse because of the small mismatch between Ag and Au lattices (with lattice parameters of 4.090 and 4.080 Å for Ag and Au, respectively) [92,93]. As a result, synthesis of Au/Ag IHNDs is challenging since anisotropic overgrowth of Ag on Au seed nanoparticles requires nonuniform surface chemistry and activity on individual Au seed nanoparticles. The examples presented in Fig. 7 provide possible solutions to form Au surface patches of different chemistries/activities through the formation of IHNDs with amorphous nanodomains. For example, Au/SiO_2 IHNDs shown in Fig. 7b have Au nanoparticles with two different surface patches, i.e. one patch passivated with SiO_2 that can prevent reactants from accessing the underneath Au surface and the other patch decorated with the hydrophilic polymeric ligands (i.e. PAA_{86}) that still allow the deposition of other materials through colloidal chemistry. Such bimodal surface activities enable the anisotropic overgrowth of Ag only on the Au surface without SiO_2 passivation, leading to the formation of SiO_2/Au/Ag ternary interfaced hybrid nanostructures [32]. Selective dissolution of SiO_2 leaves the Au/Ag IHNDs in solution. Based on the similar passivation of partial Au surface with SiO_2, a method has been developed by using superparamagnetic colloidal particles as synthesis platforms and the major steps are highlighted in Fig. 13 [94]. The superparamagnetic $Fe_3O_4@SiO_2$ core–shell nanoparticles are used as colloidal substrates that offer many advantages, such as time-efficiency associated with unique magnetic separation, scalability, and high yield for the synthesis of complex nanostructures. The SiO_2 surface of the core–shell nanoparticles can be modified with 3-aminopropyltriethoxysilane (APTS) molecules to expose the amino groups to the surrounding solution. Mixing the APTS-modified $Fe_3O_4@SiO_2$ particles with citrate-stabilized Au nanoparticles leads to the attachment of the Au nanoparticles to the core–shell nanoparticles by the strong chemical affinity between Au atoms and N atoms in the amino groups (step I). Due to the difference of surface chemistry between the SiO_2 shells and the Au nanoparticles, a second layer of SiO_2 can be selectively deposited on the original SiO_2 shells with applying a

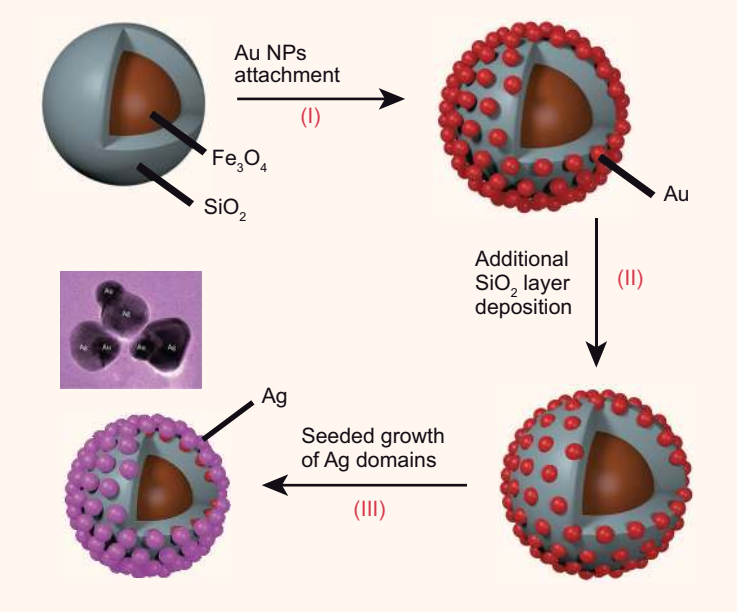

Figure 13. Schematic illustration of major steps involved in the synthesis of Au/Ag IHNDs on the superparamagnetic colloidal substrate: (I) attachment of seed Au nanoparticles on the surface of a superparamagnetic Fe_3O_4@SiO_2 core–shell colloidal substrate through chemical adsorption of Au nanoparticles to the amino groups pre-grafted on the SiO_2 surface; (II) selective deposition of a second layer of SiO_2 on the original SiO_2 shell to partially embed the Au seed nanoparticles in the SiO_2 matrix; (III) epitaxial overgrowth of Ag nanodomains on the exposed surfaces of the Au seeds. The resulting Au/Ag IHNDs can be released from the colloidal substrate by selectively dissolving the SiO_2 matrix in a dilute NaOH aqueous solution and the leftover superparamagnetic colloidal particles can be recycled for additional synthesis. The inset represents a TEM image of the synthesized Au/Ag IHNDs. Adapted with permission from [94], Copyright 2014, Wiley-VCH Verlag GmbH & Co. KGaA, Weinheim.

modified Stöber reaction. By controlling the thickness of the second SiO_2 layer, the Au nanoparticles can be partially embedded in the SiO_2 matrix, leaving partial Au surfaces to be accessible from the surrounding solution (step II). Such partial embedding of the Au nanoparticles in the SiO_2 matrix is important at least in 2-folds: (i) the Au nanoparticles are strongly immobilized on the colloidal substrates to eliminate possible detachment in the following synthetic steps; and (ii) the local environment of the Au nanoparticles becomes asymmetric to facilitate anisotropic surface processes including surface modification, assembly, and seeded growth [95,96]. In the case of seeded growth, the exposed Au surfaces act as nucleation sites for the overgrowth of Ag domains to generate asymmetric, interfaced dimers made of crystalline Au and Ag nanodomains on the Fe_3O_4@SiO_2 colloidal substrates (step III). The size of Ag domains can be tuned by controlling the concentration of $AgNO_3$ in the plating solution. Additional selective dissolution of the SiO_2 shells releases the free-standing Au/Ag IHNDs into the solution (see the TEM image, Fig. 7). The leftover Fe_3O_4@SiO_2 colloidal particles can be recycled for a new synthesis. In addition to SiO_2, other amorphous materials, such as iron oxide, have also been demonstrated to be capable of assisting the synthesis of Au/Ag IHNDs [6].

CONCLUSIONS AND REMARKS

IHNDs made of various combinations have been successfully synthesized through colloidal chemistry. In spite of the significant progress, synthesis of IHNDs consisting of different components with interesting properties in mechanics, electronics, optics, optoelectronics, etc. still represents a very interesting and challenging research direction since forming directly contacted interfaces of different materials is expected to induce unique properties due to the strong coupling between the different nanodomains. The methods and examples discussed in the aforementioned context are successful for the specific combinations of binary components. Some of the discussed methods are potentially extended to synthesize IHNDs of other compositional combinations. For instance, forming Pickering emulsion (Fig. 6a) (or colloidosomes) [97] with assembly of colloidal nanoparticles at oil/water interfaces can expose one side of the nanoparticles to water and the other to oil. If the following overgrowth occurs only in either oil or water, IHNDs can be synthesized regardless of the combination of materials in the IHNDs. Examples reported in the literature include amorphous/amorphous SiO_2/PS IHNDs (Fig. 6b), crystalline/crystalline IHNDs of Fe_3O_4/Ag, Au/Ag, FePt/Ag, and hollow-γ-Fe_2O_3/Ag [98,99]. When the two nanodomains in individual IHNDs exhibit different etching chemistry, one nanodomain can serve as mask materials to facilitate the overgrowth of new materials only on partial surface of the other nanodomains. Selectively etching the mask nanodomains leaves the free-standing IHNDs made of new compositional combinations. Typical examples include the Au/Ag IHNDs synthesized from the Au/SiO_2 IHNDs shown in Fig. 7b and Au/Pd and Au/Pt IHNDs synthesized from the Au/SiO_2 IHNDs shown in Fig. 7c [32,33]. Both Pickering emulsion and mask-assisted anisotropic overgrowth strategies are feasible to extend to the synthesis of IHNDs made of essentially any compositional combinations if the appropriate chemistries are available for overgrowing new materials and selectively etching the masking materials.

The as-synthesized IHNDs can be converted to different IHNDs through chemical transformation of either one or two nanodomains in the dimers. For instance, the Au/Ag IHNDs synthesized through

the strategy shown in Fig. 13 can react with noble metal salts (e.g. $HAuCl_4$, Na_2PdCl_4, and Na_2PtCl_4) to convert the Ag nanodomains to hollow domains of bimetallic compositions (e.g. AuAg, PdAg, and PtAg) [94]. The Ag nanodomains in the Au/Ag IHNDs can also undergo sulfidation or selenization to form silver chalcogenide (e.g. Ag_2S or Ag_2Se), resulting in Au/Ag_2X (X = S or Se) IHNDs. The Ag_2X can be further converted to other chalcogenide (e.g. CdSe or CdS) through cation exchange reactions to form Au/CdX IHNDs [100]. This strategy has also been used to synthesize Au-nanorod/AgCdSe IHNDs by using Ag-tipped Au nanorods as starting material [101]. With exploring appropriate chemical reactions, more IHNDs are expected to be synthesized from chemical transformation of the as-synthesized IHNDs. Both direct seed-mediated heterogeneous nucleation and post-chemical transformation strategy involve complicated chemical and physical processes that are necessarily probed in real time with advanced *in situ* techniques (e.g. *in situ* synchrotron SAXS and WAXS discussed in the section 'CRYSTALLINE/CRYSTALLINE IHNDS WITH DISSIMILAR CRYSTALLINE STRUCTURES') [102]. The *in situ* measurements can provide useful information to help us understand the reaction kinetics involved in nanoparticle nucleation and growth processes, and thus better design and control the synthesis to make IHNDs with improved quality and uniformity.

As a class of emerging nanostructures, most IHNDs are still limited to take the advantage of their bimodal functions inherited from their single-component counterparts. New properties due to strong coupling between the two different nanodomains in individual IHNDs are barely explored although performance enhancement of the IHNDs compared to their corresponding single-component nanoparticles has been observed in several systems as discussed in the section 'INTRODUCTION'. As a result, precise characterization of the heterogeneous interfaces in individual IHNDs and comprehensive understanding of the interfacial behaviors are critical to reveal the coupling mechanisms that are responsible for improving the existing properties as well as discovering new properties. Theoretical modeling and calculations are expected to integrate with the discovery process to help improve fundamental understanding. The achieved information will be useful to guide design and synthesis of IHNDs with tailored properties. Systematically exploring properties of the available IHNDs and those synthesized in the future represents an urgent research direction to foster the application of the IHNDs.

ACKNOWLEDGEMENTS

The author greatly appreciates Dr Jing Bai for help in searching references.

FUNDING

This work was performed at the Center for Nanoscale Materials, a US Department of Energy Office of Science User Facility under Contract No. DE-AC02-06CH11357.

REFERENCES

1. Cobley, CM, Chen, J and Cho, EC *et al.* Gold nanostructures: a class of multifunctional materials for biomedical applications. *Chem Soc Rev* 2011; **40**: 44–56.
2. Hu, M, Chen, J and Li, ZY *et al.* Gold nanostructures: engineering their plasmonic properties for biomedical applications. *Chem Soc Rev* 2006; **35**: 1084–94.
3. Sun, Y and Xia, Y. Gold and silver nanoparticles: a class of chromophores with colors tunable in the range from 400 to 750 nm. *Analyst* 2003; **128**: 686–91.
4. Sheikholeslami, S, Jun, YW and Jain, PK *et al.* Coupling of optical resonances in a compositionally asymmetric plasmonic nanoparticle dimer. *Nano Lett* 2010; **10**: 2655–60.
5. Savage, KJ, Hawkeye, MM and Esteban, R *et al.* Revealing the quantum regime in tunneling plasmonics. *Nature* 2012; **491**: 574–7.
6. Sun, Y, Foley, JJ and Peng, S *et al.* Interfaced metal heterodimers in the quantum size regime. *Nano Lett* 2013; **13**: 3958–64.
7. Mokari, T, Rothenberg, E and Popov, I *et al.* Selective growth of metal tips onto semiconductor quantum rods and tetrapods. *Science* 2004; **304**: 1787–90.
8. Mokari, T, Sztrum, CG and Salant, A *et al.* Formation of asymmetric one-sided metal-tipped semiconductor nanocrystal dots and rods. *Nat Mater* 2005; **4**: 855–63.
9. Sheldon, MT, Trudeau, PE and Mokari, T *et al.* Enhanced semiconductor nanocrystal conductance via solution grown contacts. *Nano Lett* 2009; **9**: 3676–82.
10. Steiner, D, Mokari, T and Banin, U *et al.* Electronic structure of metal-semiconductor nanojunctions in gold CdSe nanodumbbells. *Phys Rev Lett* 2005; **95**: 056805.
11. Shaviv, E, Schubert, O and Alves-Santos, M *et al.* Absorption properties of metal-semiconductor hybrid nanopareticles. *ACS Nano* 2011; **6**: 4712–9.
12. Costi, R, Cohen, G and Salant, A *et al.* Electrostatic force microscopy study of single Au-CdSe hybrid nanodumbbells: evidence for light-induced charge separation. *Nano Lett* 2009; **9**: 2031–9.
13. Costi, R, Saunders, AE and Elmalem, E *et al.* Visible light-induced charge retention and photocatalysis with hybrid CdSe-Au nanodumbbells. *Nano Lett* 2008; **8**: 637–41.
14. Yu, H, Chen, M and Rice, PM *et al.* Dumbbell-like bifunctional Au-Fe_3O_4 nanoparticles. *Nano Lett* 2005; **5**: 379–82.

15. Lin, FH and Doong, RA. Bifunctional Au-Fe_3O_4 heterostructures for magnetically recyclable catalysis of nitrophenol reduction. *J Phys Chem C* 2011; **115**: 6591–8.
16. Lee, Y, Garcia, MA and Huls, NAF *et al.* Synthetic tuning of the catalytic properties of Au-Fe_3O_4 nanoparticles. *Angew Chem Int Ed* 2010; **49**: 1271–4.
17. Sun, X, Guo, S and Liu, Y *et al.* Dumbbell-like PtPd-Fe_3O_4 nanoparticles for enhanced electrochemical detection of H_2O_2. *Nano Lett* 2012; **12**: 4859–63.
18. Sun, X, Guo, S and Chung, CS *et al.* sensitive H_2O_2 assay based on dumbbell-like PtPd-Fe_3O_4 nanoparticles. *Adv Mater* 2013; **25**: 132–6.
19. Yin, H, Wang, C and Zhu, H *et al.* Colloidal deposition synthesis of supported gold nanocatalysts based on Au-Fe_3O_4 dumbbell nanoparticles. *Chem Commun* 2008; **44**: 4357–9.
20. Wang, C, Dimon, H and Sun, S. Dumbbell-like Pt-Fe_3O_4 nanoparticles and their enhanced catalysis for oxygen reduction reaction. *Nano Lett* 2009; **9**: 1493–6.
21. LaMer, VK and Dinegar, RH. Theory, production and mechanism of formation of monodispersed hydrosols. *J Am Chem Soc* 1950; **72**: 4847–54.
22. Takahara, YK, Ikeda, S and Ishino, S *et al.* Asymmetrically modified silica particles: a simple particulate surfactant for stabilization of oil droplets in water. *J Am Chem Soc* 2005; **127**: 6271–5.
23. Qiang, W, Wang, Y and He, P *et al.* Synthesis of asymmetric inorganic/polymer nanocomposite particles via localized substrate surface modification and miniemulsion polymerization. *Langmuir* 2008; **24**: 606–8.
24. Pickering, SU. Emulsions. *J Chem Soc Trans* 1907; **91**: 2001–21.
25. Yin, Y, Zhou, S and You, B *et al.* Facile fabrication and self-assembly of polystyrene-silica asymmetric colloid spheres. *J Polym Sci Part A: Polym Chem* 2011; **49**: 3272–9.
26. Reculusa, S, Poncet-Legrand, C and Perro, A *et al.* Hybrid dissymmetrical colloidal particles. *Chem Mater* 2005; **17**: 3338–44.
27. Desert, A, Chaduc, I and Fouilloux, S *et al.* High-yield preparation of polystyrene/silica clusters of controlled morphology. *Polym Chem* 2012; **3**: 1130–2.
28. Perro, A, Duguet, E and Lambert, O *et al.* A chemical synthetic route towards "colloidal molecules". *Angew Chem Int Ed* 2009; **48**: 361–5.
29. Feyen, M, Weidenthaler, C and Schuth, F *et al.* Regioselectively controlled synthesis of colloidal mushroom nanostructures and their hollow derivatives. *J Am Chem Soc* 2010; **132**: 6791–9.
30. Lu, W, Chen, M and Wu, L. One-step synthesis of organic-inorganic hybrid asymmetric dimer particles via miniemulsion polymerization and functionalization with silver. *J Colloid Interf Sci* 2008; **328**: 98–102.
31. Chen, T, Yang, M and Wang, X *et al.* Controlled assembly of eccentrically encapsulated gold nanoparticles. *J Am Chem Soc* 2008; **130**: 11858–9.
32. Chen, T, Chen, G and Xing, S *et al.* Scalable route to Janus Au-SiO_2 and ternary Ag-Au-SiO_2 nanoparticles. *Chem Mater* 2010; **22**: 3826–8.
33. Crane, CC, Tao, J and Wang, F *et al.* Mask-assisted seeded growth of segmented metallic heteronanostructures. *J Phys Chem C* 2014; **118**: 28134–42.
34. Ohnuma, A, Cho, EC and Camargo, PHC *et al.* A facile synthesis of asymmetric hybrid colloidal particles. *J Am Chem Soc* 2009; **131**: 1352–3.
35. Ohnuma, A, Cho, EC and Jiang, M *et al.* Metal-polymer hybrid colloidal particles with an eccentric structure. *Langmuir* 2009; **25**: 13880–7.
36. She, ZW, Liu, S and Zhang, SY *et al.* Anisotropic growth of titania onto various gold nanostructures: synthesis, theoretical understanding, and optimization for catalysis. *Angew Chem Int Ed* 2011; **50**: 10140–3.
37. She, ZW, Liu, S and Low, M *et al.* Janus Au-TiO_2 photocatalysts with strong localization of plasmonic near-fields for efficient visible-light hydrogen generation. *Adv Mater* 2012; **24**: 2310–4.
38. Peng, S, Lei, C and Ren, Y *et al.* Plasmonic/magnetic bifunctional nanoparticles. *Angew Chem Int Ed* 2011; **50**: 3158–63.
39. Peng, S, Wang, C and Xie, J *et al.* Synthesis and stabilization of monodisperse Fe nanoparticles. *J Am Chem Soc* 2006; **128**: 10676–7.
40. Choi, H, Ko, SJ and Choi, Y *et al.* Versatile surface plasmon resonance of carbon-dot-supported silver nanoparticles in polymer optoelectronic devices. *Nat Photonics* 2013; **7**: 732–8.
41. Shen, L, Chen, M and Hu, L *et al.* Growth and stabilization of silver nanoparticles on carbon dots and sensing application. *Langmuir* 2013; **29**: 16135–40.
42. Choi, Y, Ryu, GH and Min, SH *et al.* Interface-controlled synthesis of heterodimeric silver-carbon nanoparticles derived from polysaccharides. *ACS Nano* 2014; **8**: 11377–85.
43. Liu, M and Chen, W. Green synthesis of silver nanoclusters supported on carbon nanodots: enhanced photoluminescence and high catalytic activity for oxygen reduction reaction. *Nanoscale* 2013; **5**: 12558–64.
44. Rao, T, Dong, XH and Katzenmeyer, BC *et al.* High-fidelity fabrication of Au-polymer Janus nanoparticles using a solution template approach. *Soft Matter* 2012; **8**: 2965–71.
45. He, J, Perez, T and Zhang, P *et al.* A general approach to synthesize asymmetric hybrid nanoparticles by interfacial reactions. *J Am Chem Soc* 2012; **134**: 3639–42.
46. McDaniel, H and Shim, M. Size and growth rate dependent structural diversification of Fe3O4/CdS anisotropic nanocrystal heterostructures. *ACS Nano* 2009; **3**: 434–40.
47. Shi, W, Zeng, H and Sahoo, Y *et al.* A general approach to binary and ternary hybrid nanocrystals. *Nano Lett* 2006; **6**: 875–81.
48. Kwon, SG, Krylova, G and Phillips, PJ *et al.* Heterogeneous nucleation and shape transformation of multicomponent metallic nanostructures. *Nat Mater* 2015; **14**: 215–23.
49. Matthews, JW and Blakeslee, AE. Defects in epitaxial multilayers. *J Cryst Growth* 1974; **27**: 118–25.
50. Gallezot, P and Richard, D. Selective hydrogenation of a,b-unsaturated aldehydes. *Catal Rev* 1998; **40**: 81–126.
51. Pellegrino, T, Fiore, A and Carlino, E *et al.* Heterodimers based on $CoPt_3$-Au nanocrystals with tunable domain size. *J Am Chem Soc* 2006; **128**: 6690–8.
52. Choi, JS, Jun, YW and Yeon, SI *et al.* Biocompatible heterostructured nanoparticles for multimodal biological detection. *J Am Chem Soc* 2006; **128**: 15982–3.
53. Lim, SI, Varon, M and Ojea-Jimenez, I *et al.* Pt nanocrystal evolution in the presence of Au(III) salts at room temperature: spontaneous formation of AuPt heterodimers. *J Mater Chem* 2011; **21**: 11518–23.
54. Kristian, N and Wang, X. Pt shell-Au core/C electrocatalyst with a controlled shell thickness and improved Pt utilization for fuel cell reactions. *Electrochem Commun* 2008; **10**: 12–5.
55. Lim, B, Kobayashi, H and Yu, T *et al.* Synthesis of Pd-Au bimetallic nanocrystals via controlled overgrowth. *J Am Chem Soc* 2010; **132**: 2506–7.
56. Njoki, PN, Lutz, P and Wu, W *et al.* Exploiting core-shell and core-alloy interfaces for asymmetric growth of nanoparticles. *Chem Commun* 2012; **48**: 10449–51.
57. Shviro, M and Zitoum, D. Tip enhanced silver growth on shaped controlled nickel nanocrystals. *J Phys Chem C* 2014; **118**: 10455–62.
58. Chen, S, Jenkins, SV and Tao, J *et al.* Anisotropic seeded growth of Cu-M (M = Au, Pt, or Pd) bimetallic nanorods with tunable optical and ctalytic properties. *J Phys Chem C* 2013; **117**: 8924–32.
59. Wang, D and Li, Y. One-pot protocol for Au-based hybrid magnetic nanostructures via a noble-metal-induced reduction process. *J Am Chem Soc* 2010; **132**: 6280–1.

60. Pacholski, C, Kornowski, A and Weller, H. Site-specific photodeposition of silver on ZnO nanorods. *Angew Chem Int Ed* 2004; **43**: 4774–7.
61. Casavola, M, Grillo, V and Carlino, E *et al.* Topologically controlled growth of magnetic-metal-functionalized semiconductor oxide nanorods. *Nano Lett* 2007; **7**: 1386–95.
62. Cao, SW, Fang, J and Shahjamali, MM *et al. In situ* growth of Au nanoparticles on Fe_2O_3 nanocrystals for catalytic applications. *CrystEngComm* 2012; **14**: 7229–35.
63. Jiang, J, Gu, H and Shao, H *et al.* Bifunctional Fe_3O_4-Ag heterodimer nanoparticles for two-photon fluorescence imaging and magnetic manipulation. *Adv Mater* 2008; **20**: 4403–7.
64. Li, Y, Zhang, Q and Nurmikko, AV *et al.* Enhanced magnetooptical response in dumbbell-like Ag-$CoFe_2O_4$ nanoparticle pairs. *Nano Lett* 2005; **5**: 1689–92.
65. Fan, FR, Ding, Y and Liu, DY *et al.* Facet-selective epitaxial growth of heterogeneous nanostructures of semiconductor and metal: ZnO nanorods on Ag nanocrystals. *J Am Chem Soc* 2009; **131**: 12036–7.
66. Ye, X, Hickey, DR and Fei, J *et al.* Seeded growth of metal-doped plasmonic oxide heterodimer nanocrystals and their chemical transformation. *J Am Chem Soc* 2014; **136**: 5106–15.
67. Wang, C, Yin, H and Dai, S *et al.* A general approach to noble metal-metal oxide dumbbell nanoparticles and their catalytic application for CO oxidation. *Chem Mater* 2010; **22**: 3277–82.
68. Wang, C, Wei, Y and Jiang, H *et al.* Tug-of-war in nanoparticles: competitive growth of Au on Au-Fe_3O_4 nanoparticles. *Nano Lett* 2009; **9**: 4544–7.
69. Lopes, G, Vargas, JM and Sharma, SK *et al.* Ag-Fe_3O_4 dimer colloidal nanoparticles: synthesis and enhancement of magnetic properties. *J Phys Chem C* 2010; **114**: 10148–52.
70. Figuerola, A, Fiore, A and Corato, RD *et al.* One-pot synthesis and characterization of size-controlled bimagnetic FePt-Iron oxie heterodimer nanocrystals. *J Am Chem Soc* 2008; **130**: 1477–87.
71. Menagen, G, Macdonald, JE and Shemesh, Y *et al.* Au growth on semiconductor nanorods: photoinduced versus thermal growth mechanisms. *J Am Chem Soc* 2009; **131**: 17406–11.
72. Carbone, L, Jakab, A and Khalavka, Y *et al.* Light-controlled one-sided growth of large plasmonic gold domains on quantum rods observed on the single particle level. *Nano Lett* 2009; **9**: 3710–4.
73. Carbone, L, Kudera, S and Giannini, C *et al.* Selective reaction on the tips of colloidal semiconductor nanorods. *J Mater Chem* 2006; **16**: 3952–6.
74. Chakrabortty, S, Yang, JA and Tan, YM *et al.* Asymmetric dumbbells from selective deposition of metals on seeded semiconductor nanorods. *Angew Chem Int Ed* 2010; **49**: 2888–92.
75. Schlicke, H, Ghosh, D and Fong, LK *et al.* Selective placement of faceted metal tips on semiconductor nanorods. *Angew Chem Int Ed* 2013; **52**: 980–2.
76. Habas, SE, Yang, P and Mokari, T. Selective growth of metal and binary metal tips on CdS nanorods. *J Am Chem Soc* 2008; **130**: 3294–5.
77. Lin, ZH, Lin, YW and Lee, KH *et al.* Selective growth of gold nanoparticles onto tellurium nanowires via a green chemical route. *J Mater Chem* 2008; **18**: 2569–72.
78. Yang, J, Elim, HI and Zhang, Q *et al.* Rational synthesis, self-assembly, and optical properties of PbS-Au heterogeneous nanostructures via preferential deposition. *J Am Chem Soc* 2006; **128**: 11921–6.
79. Yang, J, Peng, J and Zhang, Q *et al.* One-step synthesis and characterization of gold-hollow PbSx hybrid nanoparticles. *Angew Chem Int Ed* 2009; **48**: 3991–5.
80. Yang, J and Ying, JY. Nanocomposites of Ag_2S and noble metals. *Angew Chem Int Ed* 2011; **50**: 4637–43.
81. Pang, M, Hu, J and Zeng, HC. Synthesis, morphological control, and antibacterial properties of hollow/solid Ag_2S/Ag heterodimers. *J Am Chem Soc* 2010; **132**: 10771–85.
82. Lee, JS, Bodnarchuk, MI and Shevchenko, EV *et al.* 'Magnet-in-the-semiconductor' FePt-PbS and FePt-PbSe nanostructures: magnetic properties, charge transport, and magnetoresistance. *J Am Chem Soc* 2010; **132**: 6382–91.
83. He, S, Zhang, H and Delikanli, S *et al.* Bifunctional magneto-optical FePt-CdS hybrid nanoparticles. *J Phys Chem C* 2009; **113**: 87–90.
84. Buonsanti, R, Grillo, V and Carlino, E *et al.* Seeded growth of asymmetric binary nanocrystals made of a semiconductor TiO_2 rodlike section and a magnetic γ-Fe_2O_3 spherical domain. *J Am Chem Soc* 2006; **128**: 16953–70.
85. Wu, H, Chen, O and Zhuang, J *et al.* Formation of heterodimer nanocrystals: UO_2/In_2O_3 and $FePt/In_2O_3$. *J Am Chem Soc* 2011; **133**: 14327–37.
86. Cheng, C, Yu, KF and Cai, Y *et al.* Site-specific deposition of titanium oxide on zinc oxide nanorods. *J Phys Chem C* 2007; **111**: 16712–6.
87. Kwon, KW and Shim, M. γ-Fe2O3/II-VI sulfide nanocrystal heterojunctions. *J Am Chem Soc* 2005; **127**: 10269–75.
88. Kwon, KW, Lee, BH and Shim, M. Structural evolution in metal oxide/semiconductor colloidal nanocrystal heterostructures. *Chem Mater* 2006; **18**: 6357–63.
89. Gao, J, Zhang, W and Huang, P *et al.* Intracellular spatial control of fluorescent magnetic nanoparticles. *J Am Chem Soc* 2008; **130**: 3710–1.
90. Kudera, S, Carbone, L and Casula, MF *et al.* Selective growth of PbSe on one or both tips of colloidal semiconductor nanorods. *Nano Lett* 2005; **5**: 445–9.
91. Halpert, JE, Porter, VJ and Zimmer, JP *et al.* Synthesis of CdSe/CdTe nanobarbells. *J Am Chem Soc* 2006; **128**: 12590–1.
92. Sun, Y, Wiley, B and Li, ZY *et al.* Synthesis and optical properties of nanorattles and multiple-walled nanoshells/nanotubes made of metal alloys. *J Am Chem Soc* 2004; **126**: 9399–406.
93. Wang, C, Peng, S and Chan, R *et al.* Synthesis of AuAg alloy nanoparticles from core/shell-structured Ag/Au. *Small* 2009; **5**: 567–70.
94. Hu, Y, Liu, Y and Li, Z *et al.* Highly asymmetric, interfaced dimers made of Au nanoparticles and bimetallic nanoshells: synthesis and photo-enhanced catalysis. *Adv Funct Mater* 2014; **24**: 2828–36.
95. Hu, Y and Sun, Y. A generic approach for the synthesis of dimer nanoclusters and asymmetric nanoassemblies. *J Am Chem Soc* 2013; **135**: 2213–21.
96. Hu, Y and Sun, Y. Stable magnetic hot spots for simultaneous concentration and ultrasensitive surface-enhanced Raman scattering detection of solution analytes. *J Am Chem Soc* 2012; **116**: 13329–35.
97. Dinsmore, AD, Hsu, MF and Nikolaides, MG *et al.* Colloidosomes: selectively permeable capsules composed of colloidal particles. *Science* 2002; **298**: 1006–9.
98. Gu, H, Yang, Z and Gao, J *et al.* Heterodimers of nanoparticles: formation at a liquid-liquid interface and particle-specific surface modification by functional molecules. *J Am Chem Soc* 2005; **127**: 34–5.
99. Pan, Y, Gao, J and Zhang, B *et al.* Colloidosome-based synthesis of a multifunctional nanostructure of silver and hollow iron oxide nanoparticles. *Langmuir* 2009; **26**: 4184–7.
100. Weng, L, Zhang, H and Govorov, AO *et al.* Hierarchical synthesis of noncentrosymmetric hybrid nanostructures and enabled plasmon-driven photocatalysis. *Nat Commun* 2014; **5**: 4792.
101. Liang, S, Liu, XL and Yang, YZ *et al.* Symmetric and asymmetric Au-AgCdSe hybrid nanorods. *Nano Lett* 2012; **12**: 5281–6.
102. Sun, Y and Ren, Y. *In situ* synchrotron X-ray techniques for real-time probing of colloidal nanoparticle synthesis. *Part Part Syst Charact* 2013; **30**: 399–419.